PHENIX Beam Use Proposal
Run-15 and Run-16

Submitted May 29, 2014

Executive Summary

The PHENIX Collaboration is just completing two excellent data taking runs with high statistics p+p at 510 GeV in Run-13 and Au+Au at 200 GeV in Run-14. In this document we propose an exciting physics program for Run-15 and Run-16 enabled by new detector upgrades, new machine capabilities, and new theoretical developments. Our beam use request is specified in terms of recorded or trigger sampled integrated luminosity by the PHENIX experiment within a particular z-vertex window, with our best estimate of the number of weeks required to reach that goal obtained following the C-AD guidance [1]. The beam use proposal charge (included as Appendix A) requested a plan for 22 cryo-weeks in both Run-15 and Run-16. The PHENIX collaboration request is as follows.

Run-15 Proposal (22 cryo-weeks)

- p+p @ 200 GeV with transverse polarization for 9 weeks [Physics driven goal is 50 pb^{-1} recorded within $|z| < 40$ cm and $\langle \mathcal{P} \rangle = 60\%$]
- p+Au @ 200 GeV with transverse polarization of the proton for 5 weeks [Physics driven goal is 190 nb^{-1} sampled within $|z| < 40$ cm and $\langle \mathcal{P} \rangle = 60\%$. We note that the request is with half the data switching the beams to Au+p.]
- p+Si @ 200 GeV with transverse polarization of the proton for 2 weeks [Physics driven goal is 450 nb^{-1} sampled within $|z| < 40$ cm and $\langle \mathcal{P} \rangle = 60\%$]

For Run-15 the highest priority is to obtain a substantial data set of p+p @ 200 GeV and p+Au @ 200 GeV, with the proton transversely polarized. Thus, these goals are set not in terms of weeks and rather in terms of physics sampled luminosity. We are on schedule to have the MPC-EX upgrade detector complete and ready for physics. The MPC-EX enables the measurement of direct photons and extends the kinematic coverage for neutral pions at very forward rapidity. The length of the request for p+p @ 200 GeV with transverse polarization is driven by the measurement of the direct photon A_N with the MPC-EX and open charm A_N with the silicon vertex detectors, in addition to important baseline measurements for comparison with p+A and A+A results. There is enormous excitement in the collaboration for utilizing the new capability for running polarized p+A with a short switchover time. For example, new measurements with the MPC-EX will utilize

new theoretical tools for probing gluon saturation physics with transverse polarization measurements.

We have been informed that due to the installation of a "wiggler" for the testing of Coherent electron Cooling (CeC) in Run-16, the window for running p+A is only open for Run-15. We have obeyed this constraint in our current proposal. That said, the MPC-EX program is now constrained to fit within one running period and any extended ramp-up time may result in significantly lost physics — including the very interesting measurement with protons on lighter ions. Thus, we believe that a final assessment of priorities for Run-16 to potentially include additional p+A running should not be made prematurely.

Last year, the unique ability of RHIC was highlighted in our request for a short ^{3}He+Au run, where one can directly compare with the PHENIX full suite of correlation measurements the different geometries of p+Au, d+Au, and ^{3}He+Au where one selects for intrinsically larger ε_2 and ε_3 for the latter two combinations respectively [2]. We are hopeful that this running will already occur at the end of Run-14 and is thus not explicitly requested in this proposal. In the case that the ^{3}He+Au run does not occur, we would re-visit this request for Run-15 or Run-16.

Run-16 Proposal (22 cryo-weeks)

- p+p @ 62 GeV with longitudinal polarization for 6.5 weeks [Physics driven goal is 0.8 pb^{-1} recorded within $|z| < 10$ cm and $\langle \mathcal{P} \rangle = 60\%$]
- Au+Au @ 62 GeV for 9 weeks [Physics driven goal is 0.4 nb^{-1} recorded within $|z| < 10$ cm]
- p+p @ 510 GeV for 1 week [Physics goal is driven by RHICf requirements — as detailed in their separate proposal]

For Run-16, there are a number of very exciting data taking prospects. Some of these prospects are to be further informed by expected published results from the high statistics p+p at 510 GeV (Run-13) and Au+Au at 200 GeV (Run-14) data taking. We discuss the option of further data taking in these modes in Run-16. We note that for Au+Au at 200 GeV, our full Run-14 request of 1.5 nb^{-1} recorded within $|z| < 10$ cm was obtained, and that a comparable long run in Run-16 would at most increase our statistics by 150% with accelerator improvements.

We believe the most exciting prospect for charting new physics would be a comprehensive p+p and Au+Au data set at $\sqrt{s_{NN}}$ = 62 GeV. New results from PHENIX indicate potentially exciting physics in the charm sector, and the more steeply falling charm spectra may allow more detailed studies of charm collective motion in a quark-gluon plasma formed closer to the transition temperature and thus potentially more strongly coupled. In addition, measurements in a medium at a different temperature of thermal photon yields and v_2 values would be very interesting. We note that the p+p reference running would

be done with longitudinal polarization, allowing PHENIX to measure neutral pion A_{LL} at higher x where one would expect non-zero asymmetries based on the STAR $p+p$ at 200 GeV jet results.

There is also an interesting physics opportunity to install the RHICf forward detector which would measure cross sections relevant to high energy cosmic ray experiments. The RHICf collaboration will present their physics case in a separate document, and we include here a brief summary and incorporate the required one week of running time.

Years	Beam Species and Energies	Science Goals	New Systems Commissioned
2014	15 GeV Au+Au 200 GeV Au+Au	Heavy flavor flow, energy loss, thermalization, etc. Quarkonium studies QCD critical point search	Electron lenses 56 MHz SRF STAR HFT STAR MTD
2015-16	p+p at 200 GeV p+Au, d+Au, ^{3}He+Au at 200 GeV High statistics Au+Au	Extract η/s(T) + constrain initial quantum fluctuations More heavy flavor studies Sphaleron tests Transverse spin physics	PHENIX MPC-EX Coherent e-cooling test
2017	No Run		Low energy e-cooling upgrade
2018-19	5-20 GeV Au+Au (BES-2)	Search for QCD critical point and onset of deconfinement	STAR ITPC upgrade Partial commissioning of sPHENIX (in 2019)
2020	No Run		Complete sPHENIX installation STAR forward upgrades
2021-22	Long 200 GeV Au+Au with upgraded detectors p+p, p/d+Au at 200 GeV	Jet, di-jet, γ-jet probes of parton transport and energy loss mechanism Color screening for different quarkonia	sPHENIX
2023-24	No Runs		Transition to eRHIC

Figure 1: Official BNL timeline through the mid-2020s, including a transition to an Electron Ion Collider.

Our beam use request is significantly informed by the overall timeline for running at RHIC and the broader PHENIX upgrade program of sPHENIX and an evolution to a dedicated Electron Ion Collider detector. The current schedule being used by the Laboratory is shown in Figure 1. PHENIX has a major detector upgrade plan, sPHENIX, which was reviewed in October 2012 and the review committee "strongly endorsed the science case for this program." The MIE Proposal [3] has been officially submitted to the Department of Energy and awaits CD-0 approval. Science and Cost & Schedule reviews are scheduled for this summer. If successful, the existing PHENIX detector would be removed during the 2017 shutdown and the interaction region prepared for full sPHENIX installation. Thus, the Run-16 data taking period represents a critical time to complete remaining key measurements with the existing detector capabilities.

PHENIX has submitted White Papers to the Associate Laboratory Director on proposals for physics during the Beam Energy Scan - Phase 2 and on Forward sPHENIX Upgrades for studies of p+p and p+A collisions with transversely polarized protons. These White Papers are not detailed in this document and are submitted separately.

The PHENIX collaboration has a strong interest in the future Electron Ion Collider and has documented an evolution fully utilizing the PHENIX infrastructure and sPHENIX upgrades for transforming into a world-class EIC detector built around the BaBar magnet and the sPHENIX calorimetry, as shown in Figure 2. Our submitted Letter of Intent (LOI) was reviewed in January 2014 and the report detailed that "the review team was unanimous in its praise for the LOI. It well demonstrated that [this detector] would be a good day-one detector capable of addressing almost all of the physics that can be covered by eRHIC. [This detector] also appears to be a solid foundation for future upgrades so that it can explore the full physics potentials available as eRHIC itself evolves."

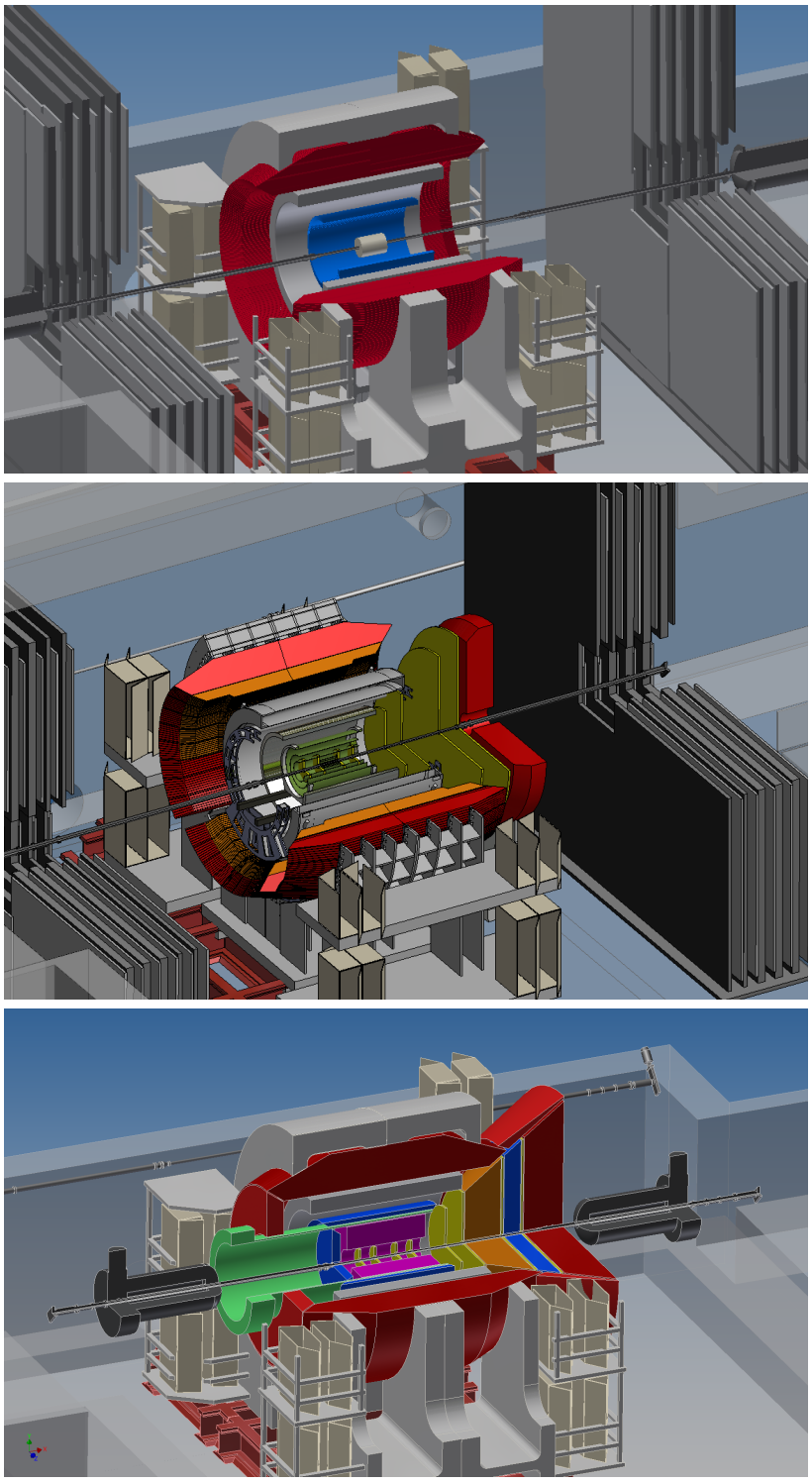

Figure 2: The evolution of the sPHENIX detector, with its focus on jets and hard probes in heavy-ion collisions, into fsPHENIX with additional instrumentation in the forward direction providing capabilities for p+p and p+A physics, and then into an EIC detector, with additional capabilities supporting its focus on e+p and e+A collisions.

Contents

Chapter 1

Recent scientific accomplishments

The PHENIX collaboration has been very productive this past year. Here we highlight a small subset of the results and detail prospects for new results in the near-term future. A strong theme amongst the results is the utilization of the unique flexibility of RHIC and the continued implementation of new PHENIX detectors and analysis techniques – for example our new dark photon search results.

1.1 Cold (or maybe not so cold) nuclear matter results

Last year we reported making a big push to fully analyze the d+Au data set including new explorations relevant to the idea of a small quark-gluon plasma being formed in these collisions. This push has resulted in the submission of many new manuscripts [4, 5, 6, 7, 8, 9, 10, 11, 12, 13] in the last year relevant to comparisons of d+Au with Au+Au data and with new p+Pb data from the LHC experiments.

Figure 1.1 (left panel) shows newly submitted results on pion and (anti) proton elliptic flow v_2 as a function of p_T in central d+Au events [5]. We highlight three key features: (1) the data are measured via correlations between our forward MPC detector and mid-rapidity tracks separated by 3 units in pseudo-rapidity thus confirming the long range nature of the correlation; (2) the mass splitting is qualitatively similar to that observed in Au+Au collisions; and (3) the overall features are reasonably described by the curves from a hydrodynamic flow calculation with $\eta/s = 1/4\pi$ following by hadronic cascade. Also shown (right panel) are comparable results from the ALICE experiment in p+Pb collisions at the LHC, indicating a somewhat lower overall v_2, though with a larger mass splitting potentially from larger radial flow. Competing explanations involving initial state effects, including glasma diagrams, are also being actively explored theoretically and we look forward to more direct data comparisons. We have published results on open heavy flavor leptons in d+Au [9] that may indicate flow pushing the heavy quarks radially outward even in these small systems [14].

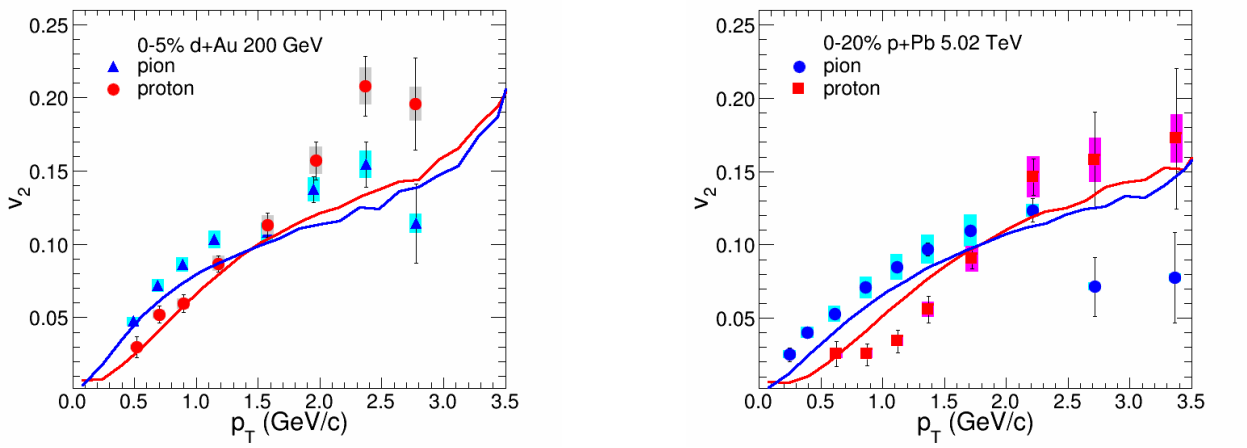

Figure 1.1: Measured $v_2(p_T)$ for identified pions and (anti)protons, each charged combined, in 0-5% central d+Au collisions at RHIC. In the left panel the data are compared with the calculation from a viscous hydrodynamic model, and in the right panel the v_2 data for pions and protons in 0-20% central p+Pb collisions at LHC from ALICE are shown for comparison.

We have also explored the space-time extent of the emission source in d+Au collisions and find a remarkable scaling of the final HBT extracted 3-dimensional radii with the initial expected size from Monte Carlo Glauber calculations [6]. The results shown in Figure 1.2 indicate that after accounting for the expected initial size, there is no significant sudden change in trends between d+Au and Au+Au, with similar conclusions utilizing LHC p+Pb data.

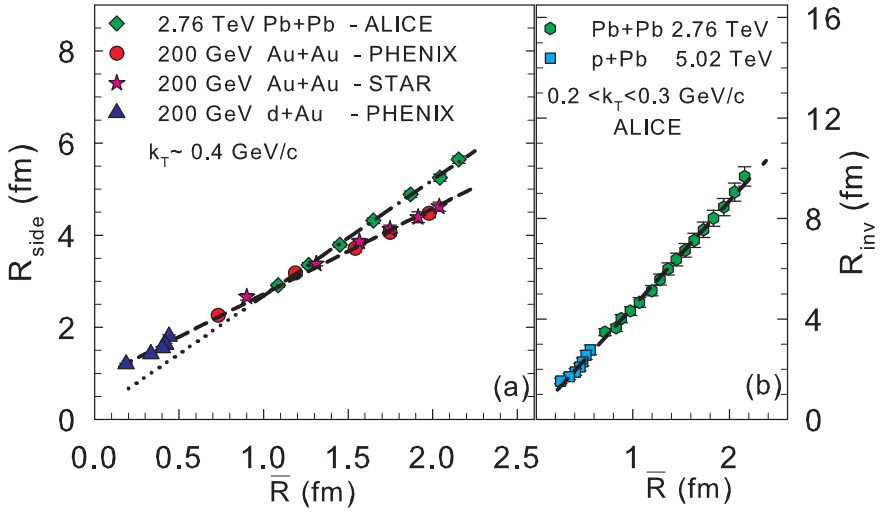

Figure 1.2: R_{side} versus $\bar{R}$ for $< k_T > \approx 0.4$ GeV/c for d+Au, Au+Au, p+Pb, and Pb+Pb collisions as indicated.

Many of these results raise good scientific questions and can be substantially advanced through p+A running and with the new PHENIX detector capabilities available for Run-15.

In particular the synergy between RHIC and the LHC results is critical for assessing competing theoretical explanations involving Color Glass Condensate glasma diagrams and collective hydrodynamics coupled to the initial geometry, pinning down the nuclear parton distribution functions particularly for gluons, and understanding other mechanisms such as initial state parton energy loss. RHIC is ideally suited to advance this scientific process of making theoretical predictions for discriminating observables and then measuring them. The case of running ^3He+Au collisions is a great example.

1.2 New geometry studies with Cu+Au and U+U

The PHENIX experiment collected excellent data sets in Run-12 with new geometry configurations of Cu+Au @ 200 GeV and U+U @ 193 GeV. We have new overall flow results for v_1, v_2, v_3, v_4, including over an extended rapidity range using the PHENIX silicon vertex detectors. We expect these results to move to publication in the next few months. We are particularly interested in the comparison of these new results with fully 3-dimensional hydrodynamic calculations.

We have also just submitted final results on J/ψ production in Cu+Au collisions [15]. Figure 1.3 (left panel) shows the ratio of J/ψ results at forward and backward rapidity, revealing a larger suppression of the J/ψ in the Cu-going direction. This additional suppression is expected due to the larger shadowing of the low-x partons from the Au nucleus, compared to the Cu nucleus, and is opposite in direction expected from hot nuclear matter effects. In the right panel we shown our preliminary U+U results which follow a similar pattern to the Au+Au results.

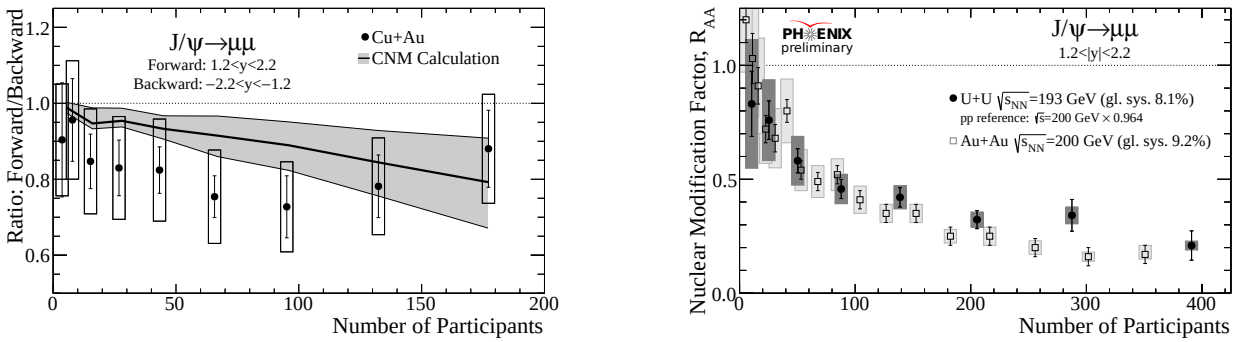

Figure 1.3: (Left panel) Ratio of J/ψ Cu+Au nuclear modifications as a function of collision participants in the Cu-going and Au-going directions. (Right panel) Comparison of J/ψ nuclear modification in U+U and Au+Au collisions.

1.3 Photons, Dark Photons, and Dileptons

The PHENIX experiment has had a strong program in photons (real and virtual) and leptons from the inception. New results shown in Figure 1.4, utilizing a novel analysis technique, confirm our earlier measurement of thermal photons and with significantly improved precision and full centrality dependence [16]. The yield and p_T distribution of this photon excess over the full centrality range is crucial for constraining models of the quark-gluon plasma photon emission. In addition, we have preliminary results to be shown on direct photon v_2 with improved precision and now also v_3. We expect to publish these results this year, and in particular the v_3 result is key to testing theoretical ideas for resolving the large photon v_2 results [17] seen at both RHIC and the LHC.

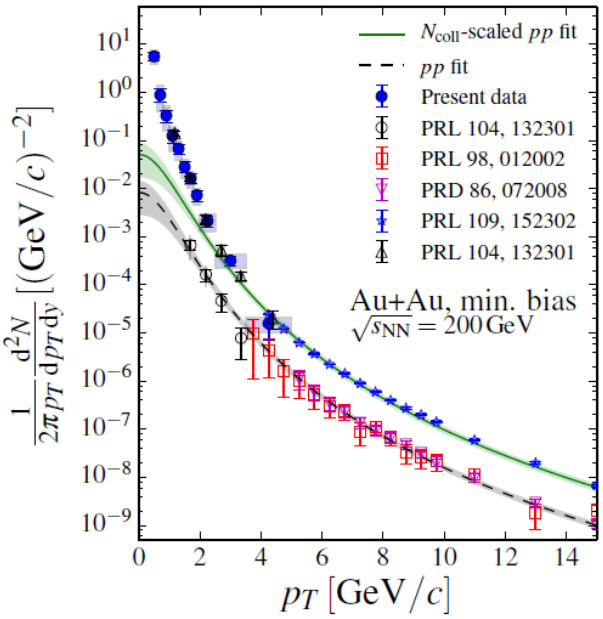

Figure 1.4: Direct photon p_T spectra for minimum bias Au+Au from this measurement (solid symbols) and Au+Au and p+p collisions (open symbols).

The PHENIX experiment has a strong tradition of utilizing the detector with new analysis techniques and new ideas arising within the collaboration. The PHENIX data set include a very large sample of neutral pion Dalitz decays and if a Dark Photon [18] exists, it should mix with the virtual photon and create an enhancement in the invariant mass distribution of the dielectron pair. The Dark Photon is a low mass, very weakly coupled candidate to explain the $g-2$ anomaly. Figure 1.5 shows our preliminary limits (since we observe no statistically significant signal), which are currently the best over portions of the mass range. We expect to publish results from these data sets in the next few months.

The PHENIX collaboration has made progress towards publication of the Run-10 Au+Au dilepton results with the Hadron Blind Detector (HBD). The HBD was constructed to confirm or refute the interesting dilepton results published by PHENIX in the challenging

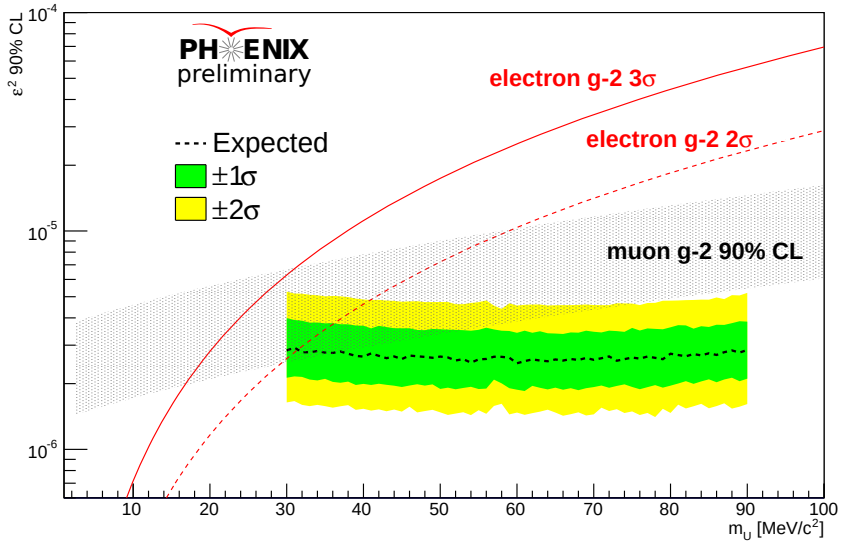

Figure 1.5: PHENIX Preliminary result on the upper limit set for Dark Photons.

low signal to background data set [19]. The recent submission of results from the STAR collaboration [20] underscores the importance of finalizing our HBD results. Two independent analysis techniques have been applied to the HBD Run-10 data set, and final results are near completion. We expect these final results to be published this year. We note that new results utilizing the HBD for single electron from open heavy flavor and for high p_T charged pion identification are near publication as well.

1.4 Closed and Open Heavy Flavor

We have also used dilepton pairs (both electron-muon pairs and dielectron pairs) to extract yields and distribution modifications of open heavy flavor. Figure 1.6 (left panel) compares the electron-muon relative azimuthal angular distribution between p+p and d+Au collisions [7]. There is a significant suppression of the back-to-back peak in d+Au collisions - which may result from shadowing reducing the total charm production and also from charm quark interactions with the d+Au produced medium thus reducing the initial angular correlation of charm and anti-charm quark. The right panel shows the dielectron distribution from d+Au collisions from an analysis fully differential in pair p_T and invariant mass [12]. This result allows for an excellent isolation of the beauty contribution and thus a relatively model independent extraction of the cross section.

We also have a submitted manuscript [21] on the yield of Upsilons in Au+Au collisions. The results shown in Figure 1.7 indicate a suppression of the three states in central Au+Au events, and within uncertainties, consistent with no contributions from the 2s and 3s states as also observed by CMS at the LHC.

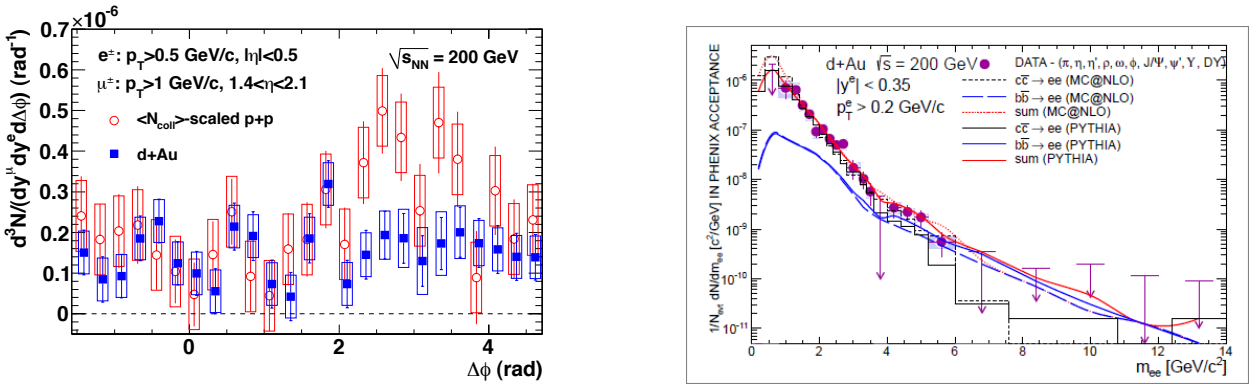

Figure 1.6: (Left panel) Electron-muon azimuthal correlations from $p+p$ and $d+$Au collisions. (Right panel) Dielectron result in $d+$Au collision and one slice of the full p_T and invariant mass fit.

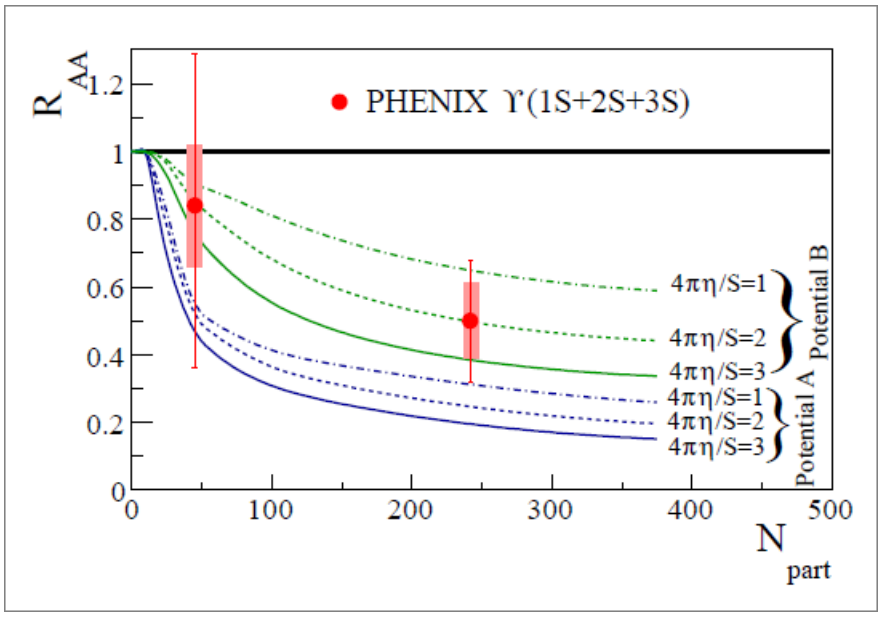

Figure 1.7: Upsilon centrality dependent R_{AA} in Au+Au collisions compared with theoretical calculations from Strickland and Bazow [22].

Run-11 was the commissioning run of the PHENIX silicon vertex barrel detector (VTX) and Run-12 for the PHENIX forward silicon detector (FVTX). The Run-11 data set for the VTX has a more limited acceptance and some detector stability issues. We believe these are now understood and expect to have a first published result in the next six months. The FVTX performance in the Run-12 Cu+Au was quite good and the analysis is rapidly progressing towards publication. These anticipated results are a major focus of the collaboration.

Details on the silicon detector performance for Run-14 are included in Section 2.2.

1.5 Spin physics results

The PHENIX experiment has high statistics neutral pion double spin asymmetries A_{LL} from the combined Run-05, Run-06, Run-09 data sets, which when considered with the STAR experimental results on reconstructed jets, give the first indication of a non-zero gluon contribution to the proton spin. The PHENIX collaboration has finalized these results and submitted them to publication [23]. Figure 1.8 shows these results and their comparison to different calculations based on fits to polarized scattering data. The focus of ΔG measurements is now moving to lower gluon momentum fraction x, which is accessible from measurements at forward rapidity measurements or/and higher center of mass collision energy. The analysis of $\sqrt{s_{NN}} = 510$ GeV data in both central and forward rapidity regions is progressing well and results are expected to be released in 2014.

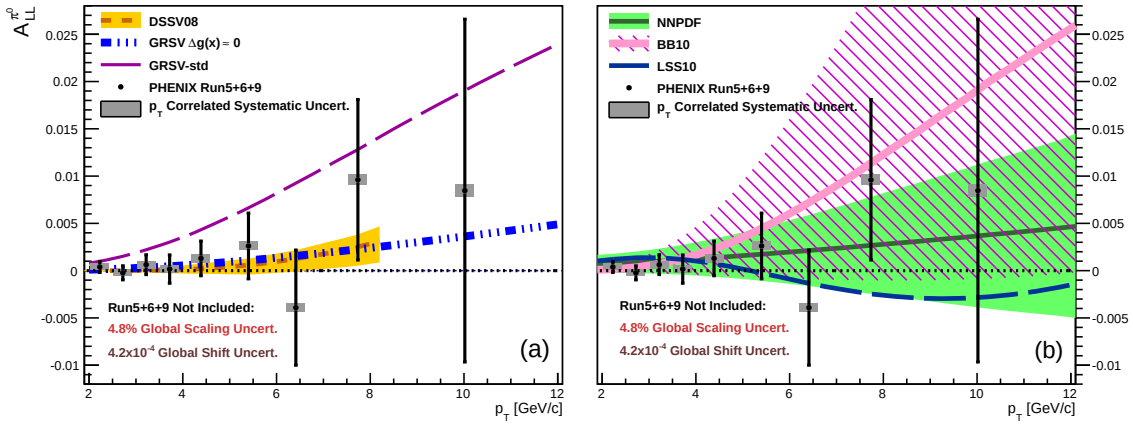

Figure 1.8: Points are the combined A_{LL} versus p_T for mesons from 2005 through 2009 with the statistical uncertainty. The p_T correlated systematic uncertainty given by the gray bands is the result of combining the year-to-year uncorrelated parts of the systematic uncertainties on relative luminosity and polarization. The year-to-year correlated parts are given in the legend. Plotted for comparison are several expectations based on ts to polarized scattering data, with uncertainties where available.

PHENIX has previously published transverse asymmetries of charged hadrons and neutral pions at mid-rapidity, the latter have been used for an upper limit of the gluon Sivers function constraint. In recent data the statistical uncertainties of this measurement have been decreased by a factor of more than 20. In the forward direction, we see that non-vanishing transverse asymmetries which have been observed at medium energies in the past ($\sqrt{s_{NN}} < 20$ GeV) persist to $\sqrt{s_{NN}} = 200$ GeV. Results on neutral pion and eta meson asymmetries in central rapidity at $\sqrt{s_{NN}} = 200$ GeV and neutral pion (cluster) asymmetries at $\sqrt{s_{NN}} = 62.4$ (200 GeV) in forward kinematics are summarized in the paper recently submitted [24]. Based on a comparison of charged and neutral pions (see Figure 1.9) we conclude that initial state effects alone cannot explain these asymmetries. Results on single spin asymmetries in eta meson production in forward rapidity are being

finalized and will be submitted to publication shortly.

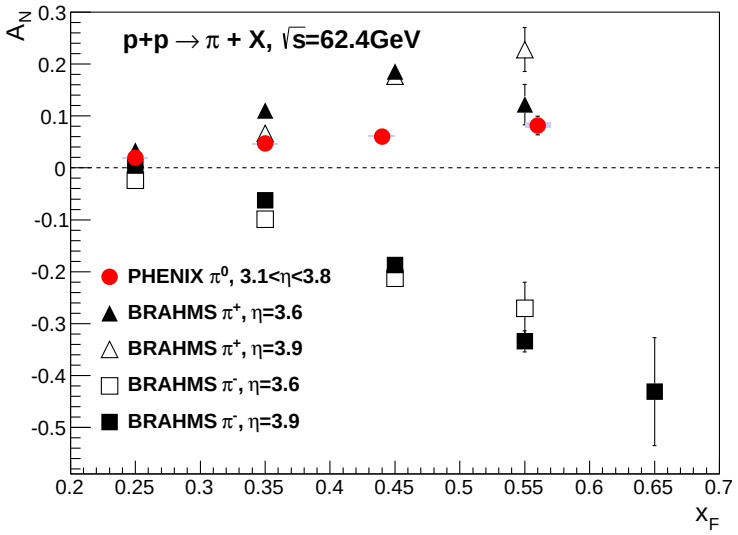

Figure 1.9: PHENIX neutral pion asymmetries compared with charge pion results from the BRAHMS experiment.

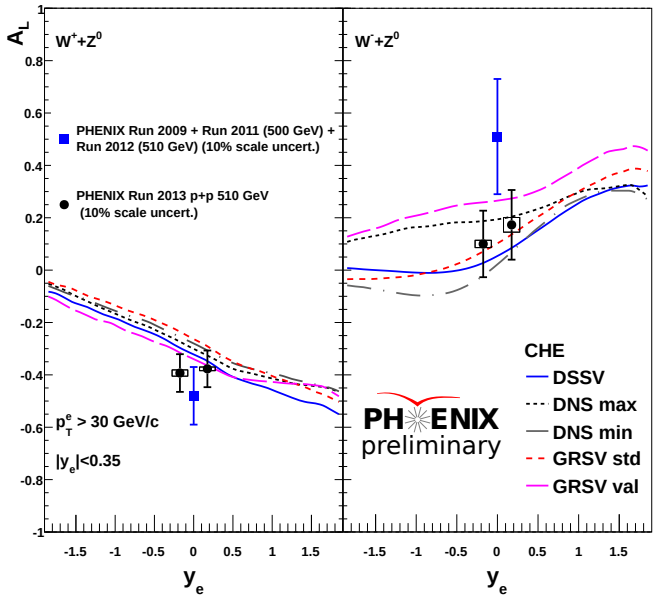

Figure 1.10: W and Z to electron single spin asymmetry as a function of lepton rapidity.

Significant progress has been made on the analyses of $W \rightarrow e$ at mid-rapidity and $W \rightarrow \mu$ at forward rapidity. Data collected in Run-13 added a factor of 2.5 more statistics to that available from previous 500 and 510 GeV Run-9, Run-11 and Run-12. This will lead to

significantly improved results, particularly for the $W \rightarrow \mu$ measurement, in which the Forward Silicon Vertex Tracker (FVTX) will considerably help with background rejection. The 2009 results of $W \rightarrow e$ decays in the PHENIX central arms were published in 2011. Results from 2011 and 2012 both from central arms and muon arms have been approved. In addition, the $W \rightarrow e$ results from Run-13 (Figure 1.10) are also "preliminary" approved and are expected to be published shortly together with Run-11 and Run-12 results.

Chapter 2

Status of upgrades

In this Chapter we report on the status of key PHENIX detector upgrade projects. The first three sections relate to the forward silicon vertex detector (FVTX), the barrel silicon vertex detector (VTX), and the Muon Piston Calorimeter Extension upgrade (MPC-EX). These three projects are directly relevant to the physics measurements and readiness for the proposed data taking in Run-15 and Run-16 of this beam use proposal. Then we detail the successful implementation and running of the Muon Trigger and Resistive Plate Chamber (RPC) upgrade for the spin W physics program as utilized in Run-13 $p+p$ @ 500 GeV running. Finally we have a brief update on smaller scale and very successful data acquisition improvements.

2.1 Forward silicon vertex detector (FVTX)

The PHENIX detector Barrel and Forward Silicon Vertex Trackers are shown in Figure 2.1. The two Forward Silicon Vertex Trackers (FVTX), which are described in detail in Ref. [25], are endcap detectors which extend the vertex capability of the VTX to forward and backward rapidities, providing space points before the absorber materials and secondary vertex measurement capability in front of the PHENIX muon arms. The FVTX detector was successfully installed into PHENIX in December 2011 and has undergone commissioning and operations during Run-12, Run-13 and Run-14. During the shutdowns following Run-12 and Run-13, FVTX electronics that became non-functional either during the run or during de-installation from the IR were repaired and FPGA codes were updated as needed. As a result, the FVTX detector has maintained an operational state of $> 95\%$ live channels for Run-13 and Run-14.

The FVTX was designed to be able to identify secondary vertices near the primary event vertex. With an expected distance of closest approach (DCA) resolution of better than 200 μm at 5 GeV/c, we can separate prompt particles from particles that have short decay distances (B and D mesons) and longer-lived particles such as pions and kaons. The

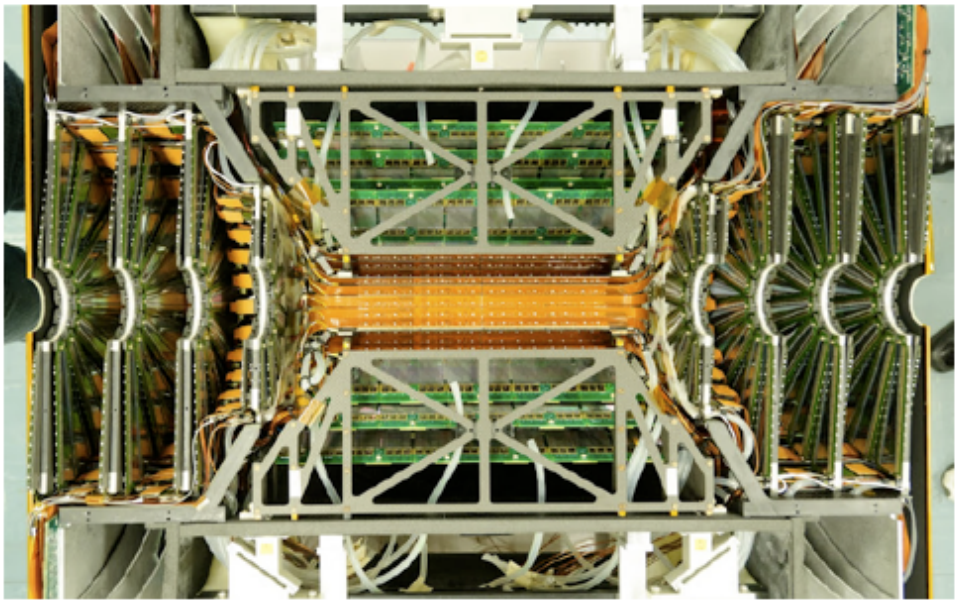

Figure 2.1: Picture of the PHENIX VTX Barrel plus FVTX End Cap Detectors.

FVTX detector improves the dimuon mass resolution by providing a better opening angle measurement than can be provided by the muon arms alone, allows for isolation cuts to help discriminate between muon signals and hadronic backgrounds, and provides further discrimination against hadronic particles which decay in the muon volume by requiring that the track passing through the FVTX planes and the muon planes have a good χ^2 fit value. With these new capabilities, we can precisely measure open heavy flavor production at forward rapidity, improve the background rejection and separation of J/ψ and ψ(2S) in the dimuon spectra, and separate Drell-Yan dimuons from dimuons produced through heavy flavor and/or hadronic decays. The FVTX detector also improves the reaction plane measurement significantly and is providing a new precision measurement of the relative bucket-to-bucket luminosities in polarized $p+p$ collisions, which is critical for PHENIX spin analyses.

In Run-12, the intrinsic performance of the FVTX detector was studied using real collision data and front-end injection calibration data, and all detector performance specifications were met, including $>$95% detector efficiency in the active area, $\sim$500 electron noise level on all readout channels, and an intrinsic detector resolution limited only by the readout pitch and multiple scattering of particles. This intrinsic detector performance has been maintained throughout each of the data taking runs. We have also analyzed Run-12 and Run-13 data and studied the track finding efficiencies, the DCA performance, the improvement to the dimuon mass resolution, the background rejection and the reaction plane resolution. We show some selected performance plots from these studies here.

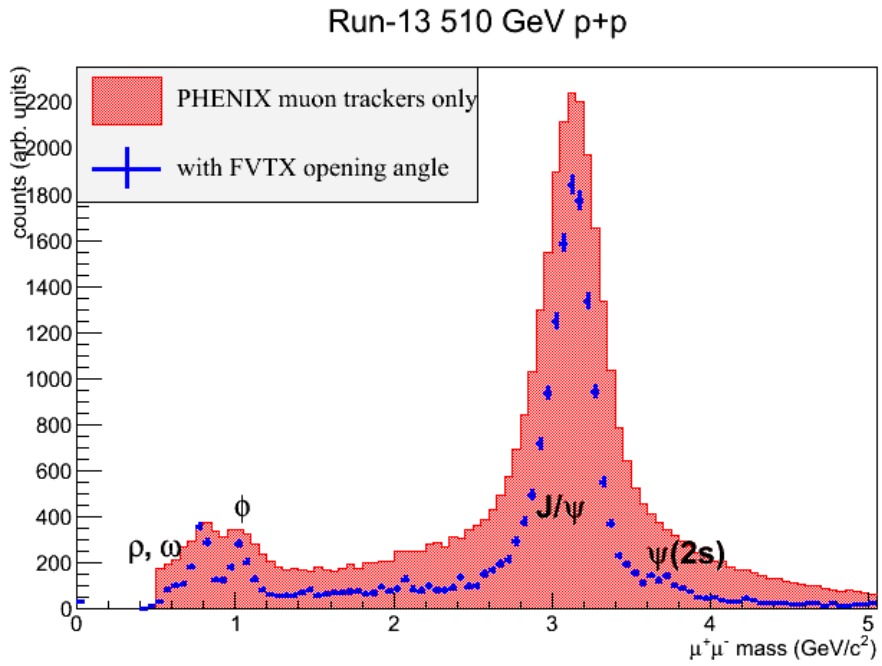

Figure 2.2: Reconstructed unlike-sign dimuons for a set of the Run-13 p+p data. Shown in red is the reconstructed mass from the muon arm alone and the blue crosses show the reconstructed mass for tracks which are matched to FVTX tracks and refit using the FVTX detector. Both histograms have been re-scaled.

Figure 2.2 shows a reconstructed dimuon mass spectrum from Run-13 p+p data for the muon arm alone (red) and, for the same data set, the combined muon and FVTX detector mass spectrum (blue crosses). Both histograms have been re-scaled. As can be seen, the FVTX improves the mass resolution significantly, especially for the ϕ, ρ, ω, J/ψ and ψ(2S) peaks and the combinatorial background is reduced as the FVTX detector rejects hadronic backgrounds. With spectra like this, we are extracting the measured J/ψ:ψ(2S) yields in Run-13 510 GeV p+p data and are working on the same for the Run-12 Cu+Au data. We have also used the FVTX detector to cleanly identify when more than one interaction has occurred during an event in 510 GeV p+p running and, if there is more than one, to determine the location of each vertex point and assign the appropriate vertex to each track. Assigning the correct vertex to a dimuon candidate is crucial to maintaining our good mass resolutions and to correctly tagging prompt and decay particles. Once the ratio analyses are completed, we will also extract absolute cross sections and perform the same analyses using the newly collected Run-14 Au+Au data set.

To achieve the DCA resolution needed to separate heavy flavor decays from hadronic backgrounds, we need to achieve precision alignment of all detector components within the FVTX and VTX detectors and then between the FVTX and VTX detectors and the beam position. Much work has gone into achieving this goal and as a result we are now able to extract DCA resolutions that are of the order that we get from simulations. An example of

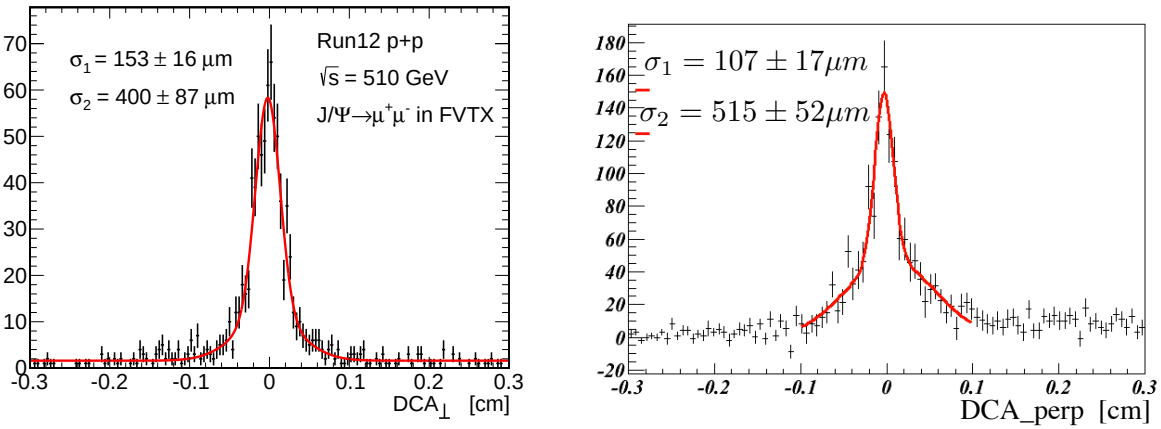

Figure 2.3: The DCA resolution extracted from Run 12 p+p data (left-hand plot) and from Run 12 Cu+Au data (right-hand plot), for muons nominally originating from J/ψ decays.

the DCA that is measured for muons nominally coming from J/ψ decays is shown Figure 2.3 where the DCA distribution for J/ψ candidates is shown for both the Run 12 p+p data and for the Run 12 Cu+Au data. Each distribution is fit to two gaussians, with the assumption that the narrower gaussian represents the actual J/ψ muons which have been correctly reconstructed and the broader gaussian represents some remaining background in the distribution. The narrower gaussians from the fits give resolutions of 100-150 μm, which is consistent with expectations.

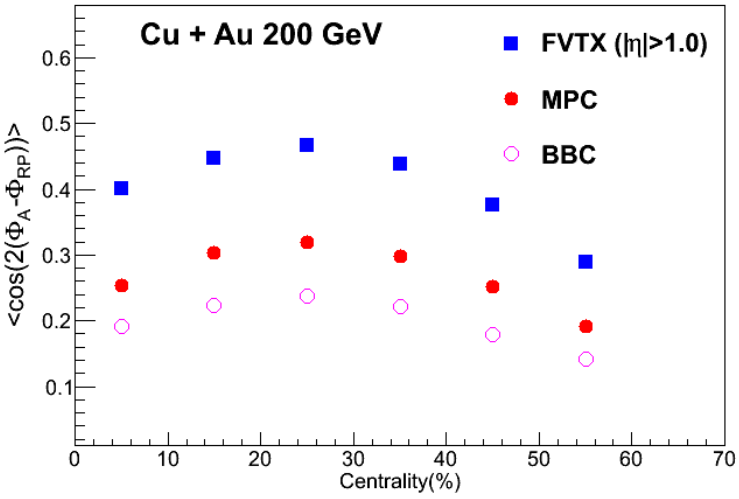

Figure 2.4: Reaction plane resolution versus centrality for the FVTX, MPC and BBC detectors, extracted from Run 12 Cu+Au data.

The FVTX detector also now provides the highest precision reaction plane from existing PHENIX detectors. An example of the reaction plane resolution achieved from Cu+Au

data, compared to that extracted from other PHENIX detectors is shown in Figure 2.4. As can be seen, the resolution from the FVTX detectors is approximately 1.5 times better than that achieved by the MPC. The FVTX detector is also currently being used to extract flow measurements from the Cu+Au data set.

The FVTX detector performance has been verified to be ready for definitive vector meson and open heavy flavor measurements in Au+Au in Run-14 as well as the already collected data sets from 510 GeV p+p and 200 GeV Cu+Au.

2.2 Barrel silicon vertex detector (VTX)

The PHENIX barrel silicon vertex detector (VTX) is a 4 layer silicon tracker. The inner two layers, B0 and B1, are made of pixel detectors and the outer two layers, B2 and B3, are made of stripixel detectors. The VTX detector was installed in the PHENIX interaction region in December, 2010 and had its first commissioning with beam and data taking in Run-11.

During Run-11, the detector had issues with the read-out electronics board for the pixel system. As a result, many of the pixel ladders were not properly read-out, which reduced the live area of the detector during the run. This problem was repaired during the shut-down after Run-11. Additionally, some of the pixel ladders were damaged in the time frame of Run-11. Wire-bonding between the pixel sensors and the read-out busses were broken. The cause of the damage was not completely understood, but the most likely cause was thermal stress. The problem has been addressed through an extensive two-year repair program and an improvement to the operating condition of the VTX that minimizes large changes to the operating temperature of the ladders. No damage of any significance has occurred to the pixel ladder wire bonds during Run-12, Run-13, and the current Run-14. The repair program involved the removal of all damaged pixel ladders from the VTX, re-bonding of these damaged ladders, and re-installing those repaired ladders into the VTX. We also installed spare ladders with improved performance. The repair program was complete ahead of the start of Run-14.

The stripixel detectors had minor read-out issues in Run-11 and Run-12 and those issues were addressed during the shutdown after each run. However, just prior to Run-13, the cooling tubes of the stripixel detector developed multiple, severe coolant leaks. The leaks were caused by galvanic corrosion of the aluminum tube. We designed and built new staves without aluminum material and rebuilt all 40 stripixel ladders by moving the silicon sensor modules from old staves to new staves. This repair program was very successful and was complete prior to the start of Run-14.

The newly rebuilt VTX detector was installed in the PHENIX interaction region for Run-14. The repairs were successful. We are now well into the run, and we have not had any significant issues in detector operation. The Run-14 data set is projected to be very good for the analysis of open charm and beauty physics.

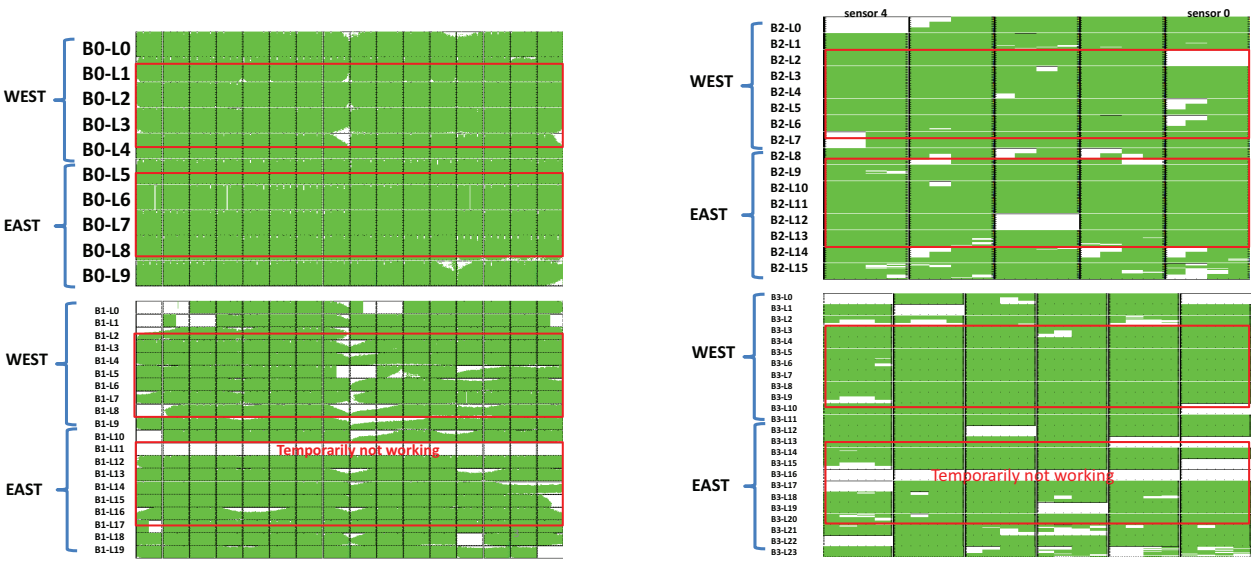

Figure 2.5: Hit map of VTX detector. The top two panels are pixel detectors (B0 layer and B1 layer) and the bottom two panels are stripixel detector (B2 and B3). The green area is the live area of the detector. The red squares indicate the acceptance of PHENIX central arms.

Figure 2.5 shows a hit map of the VTX in Run-14. The green area shows the live area. The red squares indicate the acceptance of PHENIX central arms. In the plot, one of the 30 pixel ladders, B1-L11 and one of 40 stripixel ladders, B3-L16, are not reading out properly. Both ladders were working when the VTX detector was assembled and before VTX was moved to PHENIX IR. We believe that both ladders have a problem with a poor connection internal to the detector and will be recoverable during the upcoming 2014 RHIC shutdown. Each of these two ladders causes 6 to 7% of loss of live area in the PHENIX central arm acceptance.

The fraction of live area in the PHENIX central arm acceptance is 98% in B0, 83% in B1, 95% in B2, and 84% in B3. In the data analysis, we need 2 pixel hits and at least one stripixel hit to connect an electron track reconstructed in Drift chamber to the VTX. The two pixel hits are needed for precision measurement of DCA and to veto photon conversions in the B0 layer. The point in B2 or B3 is needed to connect the DC track to the pixel tracklets. The overall efficiency of connecting DC and VTX is estimated to be $\simeq$ 80%. Our data analysis in Run-11, which has significantly larger dead area due to the issues mentioned above, demonstrated that these hit requirement can achieve DCA resolution better than 80 μm for $p_T > 1$ GeV/c with very small level of fake background that is sufficient for separating $b \rightarrow e$ and $c \rightarrow e$.

We are close to finalizing the Run-11 Au+Au data analysis, which has been more challenging due to the initial detector issues described above. The Run-12 Cu+Au data set has been reconstructed and analysis is ongoing. The Run-14 data is looks to be of very high quality and should provide our golden data set of open heavy flavor physics when combined with the projected high statistics Run-15 p+p at 200 GeV running as the baseline.

2.3 Muon piston calorimeter extension (MPC-EX)

The Muon Piston Calorimeter (MPC) Extension, or MPC-EX, is a Silicon-Tungsten preshower detector that will be installed in front of the existing PHENIX MPCs, as shown in Figure 2.6. This detector consists of eight layers of Si "minipad" sensors interleaved with tungsten absorber and enables the identification and reconstruction of prompt photons and π^0s at energies up to $\sim$ 80 GeV.

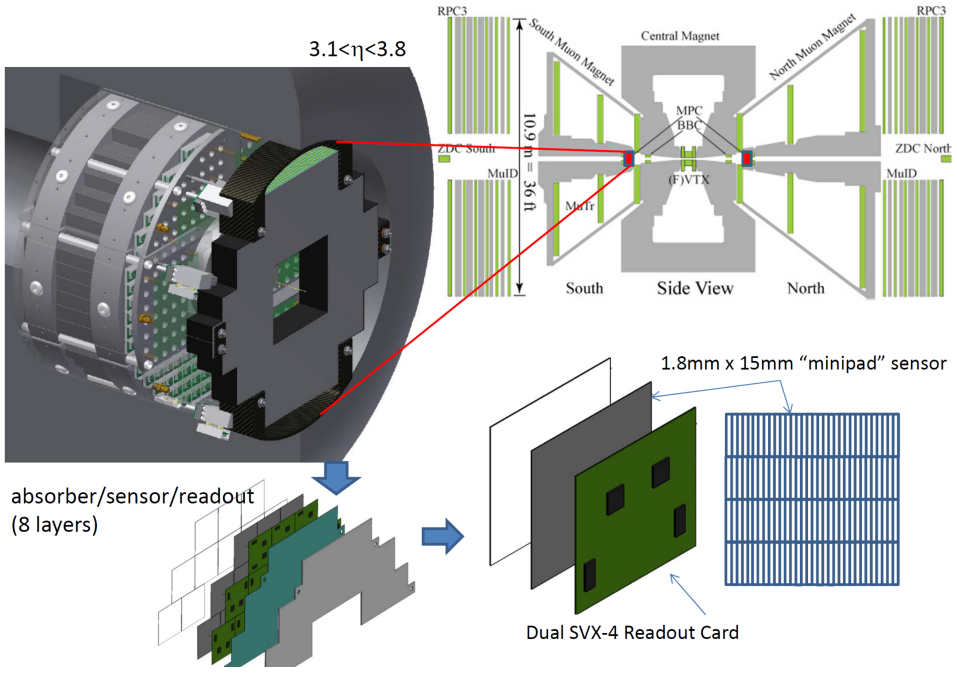

Figure 2.6: The PHENIX detector (upper right), showing the location of the existing Muon Piston Calorimeters inside the muon magnet piston. The MPC-EX (upper left) will consist of eight measurement layers of absorber, sensors and readout. The "minipad" sensors themselves (lower right) will consist of a readout card bonded to a Si sensor. The orientation of the long direction of the minipads will alternate between layers.

The MPC and MPC-EX sit at forward and backward rapidities ($3.1 < |\eta| < 3.8$) and are uniquely positioned to measure phenomena related to either low-x partons (in the target hadron or nucleus) or high-x partons (in the projectile nucleon or nucleus). We will use the capabilities of the MPC-EX to make critical new measurements that will elucidate the gluon distribution at low-x in nuclei as well as the origin of large transverse single spin asymmetries in polarized p+p collisions. The MPC-EX construction effort and schedule are on track to have both arms installed in PHENIX and ready for Physics in Run-15.

The active elements in the MPC-EX are the Si minipad sensors. The sensors are 500 μm thick and 6.2 cm $\times$ 6.2 cm in size, divided into 128 channels 1.8 mm wide by 1.5 cm in length. Each channel has a high and low gain digitization path, which allow for energy

measurements from a single MIP up to full energy electromagnetic showers. The short distance along the minipad sensors is rotated by ninety degrees for alternating layers to provide a three-dimensional high resolution image of the developing electromagnetic shower.

The sensors were jointly developed between Yonsei University and Brookhaven National Laboratory and produced at ETRI in Korea. Sensor production started in early 2014, and at the present time over half of the sensors have been produced, diced and tested at Yonsei and Iowa State. Sensor yield is >70%, and leakage currents are less that 1μA. Sensor production is expected to be completed by July 2014.

In addition to the sensors themselves, the Si micromodules consist of a sensor bonded to a dual-SVX readout card (ROC). The ROCs (designed by ISU and BNL) have been seen two rounds of prototypes, and production ROCs are being populated. Each ROC has two SVX4 custom ASICs for digitization and readout (high and low gain channels). The SVX4.2b ASICs were manufactured in a special production through MOSIS/TSMC and are behaving identically to previously produced chips.

The micromodules for the MPC-EX plug into a "carrier board" – see Figure 2.6. Each carrier board has two readout chains of six micromodules. The carrier board has been designed, prototype testing is complete, and production boards are on order. Because the SVX4s handle digitization and are read out in a serial "daisy chain" fashion, the FEM required to interface them to the PHENIX DAQ is relatively simple. The readout chain for the MPC-EX was verified using protype FEM readout boards, both on the bench and in the FNAL sPHENIX test beam where Si strip modules were used as a beam hodoscope. The FEM design is complete, and production board are on order.

During the summer of 2013 the MPC-EX group placed a collection of 25 MPC crystals in a test beam at FNAL. The primary goal of this test beam was to characterize the response of the MPC APDs to charged particles. Because the MPC APDs sit on the front of the detector they will be exposed to the partially developed shower when the MPC-EX is in place. Understanding the sensitivity of the APDs to charged particles is important to understanding the overall operation of the combined MPC and MPC-EX detectors. Results from the test beam showed that the APD MIP response was as expected for the particular model of APD, and consistent with previous measurements from CMS. A second beam test is planned for late June, 2014, at SLAC using electron beams. This beam test will include the MPC-EX preshower in front of the MPC crystal array, with the goal of demonstrating the ability to reconstruct closely spaced electromagnetic showers.

The MPC-EX group has also installed three carrier boards (each with three prototype micromodules) in front the south MPC during Run-14, as shown in Figure 2.7. The purpose of this installation is to gain experience with the detector operating in the PHENIX muon piston so that systems integration issues such as noise, temperature stability, etc., can be investigated and solved prior to the full installation for Run-15. Initial results show that the temperature in the magnet piston is stably 1^{o}C higher with the MPC-EX installed, consistent with expectations. The installed detector has been read out into the PHENIX

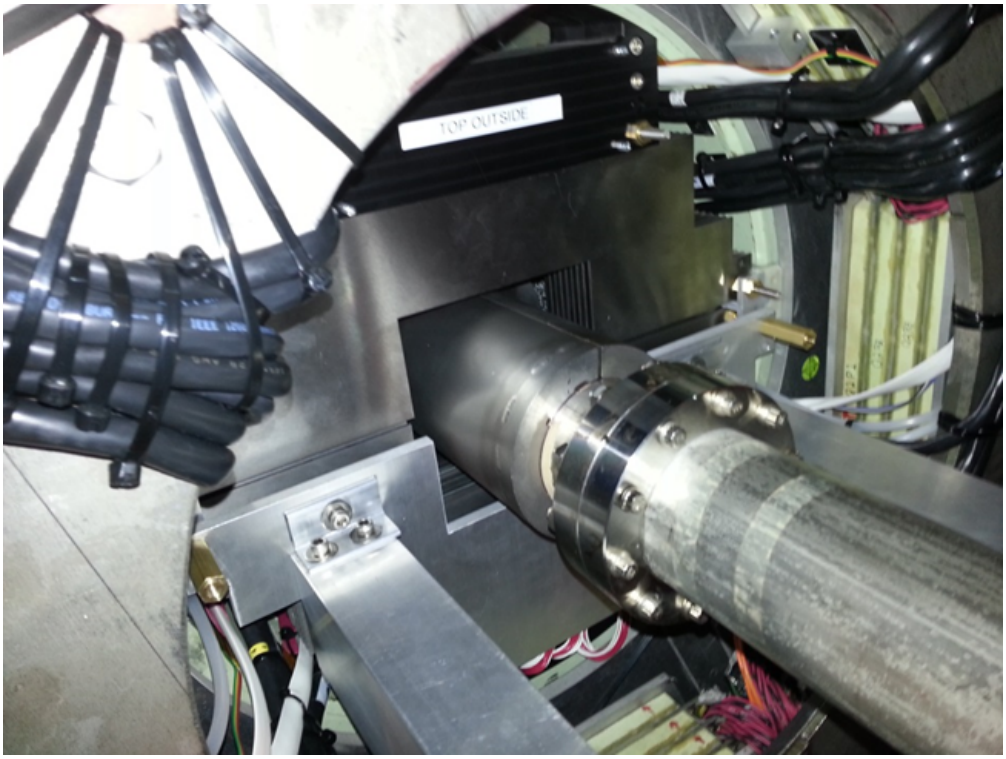

Figure 2.7: The Run-14 MPC-EX installed in the PHENIX south muon magnet pit. The installation fixture, still attached, is visible in the bottom half of the picture.

DAQ as a standalone detector, and work is ongoing to integrate the Run-14 prototype into the full PHENIX readout partition. The Run-14 prototype is also being used as a test bed to develop the online monitoring software and raw data decoding chain that will be used for the full detector.

The MPC-EX group has made great strides in the past year in moving from prototyping to production, and developing the hardware and software infrastructure to operate the detector efficiently. At the present time we see no technical or schedule impediments to installing both MPC-EX arms and being ready for physics in time for RHIC Run-15.

2.4 Muon trigger system

The PHENIX *W* physics program relies on upgrades of the muon system in order to be able to trigger on high momentum muons. This system has two principal components which were commissioned before and during 2012. Additional trigger cards for the front-end electronics of the muon tracking chambers (MuTr) provide the necessary capabilities to include the muon tracker information (SG1) in the trigger chain (funded by the Japan Society for the Promotion of Science). Resistive plate chambers (RPC) in front of (RPC1) and behind (RPC3) the existing muon arm detectors combine additional track information

with good timing resolution for the trigger system (funded by the U.S. National Science Foundation). This trigger mix demonstrated sufficient rejection power in Run-13 keeping trigger rate below the bandwidth limit of PHENIX DAQ system and sampling the full luminosity.

The trigger efficiencies of SG1 triggers are shown in Figure 2.8. The efficiencies were evaluated for South and North trigger mix SG1xBBCLL1 using various trigger (ERT, MPC, MinBias, MUID1D) event samples with transverse momentum above 5 GeV/c. From intensive studies so far, we know these trigger efficiencies tend to become low if hadron background are contaminated in the event samples. In order to present the real efficiencies for muons from W decay as much as possible, W likelihood ratio of above 0.9 are selected. The efficiencies achieved were above $\sim 80\%$ for these event samples.

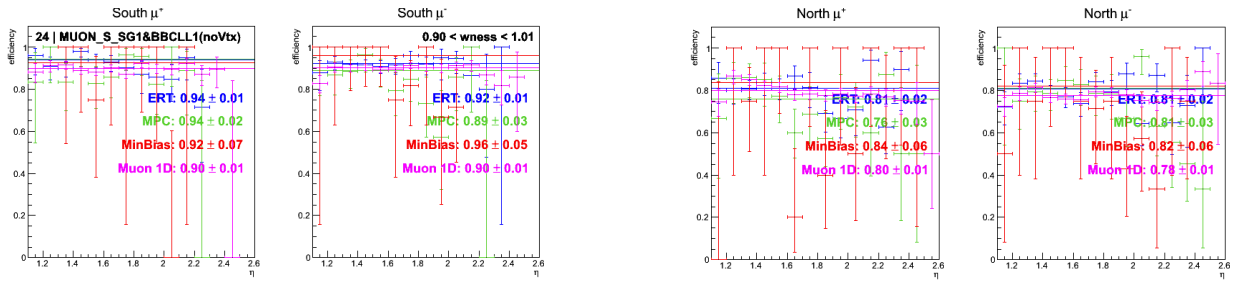

Figure 2.8: Trigger efficiencies of the trigger mix of SG1xBBCLL1 for various trigger samples plotted as a function of rapidity. Top shows these of South and bottom shows North.

Overall the muon trigger upgrade system performed very well during the high luminosity Run-13 $p+p$ at 510 GeV data taking. This resulted in a high statistics sample for the W analysis.

2.5 Data Acquisition Upgrades

Several different modest upgrades in the PHENIX data acquisition system have led to unprecedented performance figures in Run-14. We have achieved, in Au+Au at 200 GeV, event rates of 6 kHz at a live time of about 90%. Note that last year's Beam Use Proposal assumed a conservative 5 kHz rate for these heavy ion collisions. This overall performance is shown in the left panel of Figure 2.9.

The main upgrades consisted of

- Firmware changes for the Global Level 1 (GL1) trigger,
- Replacement of back end CPUs with newer faster machines,
- Optimized tuning of the main network switch,

- Expansion of the switch with componentns from the RHIC Computing Facility.

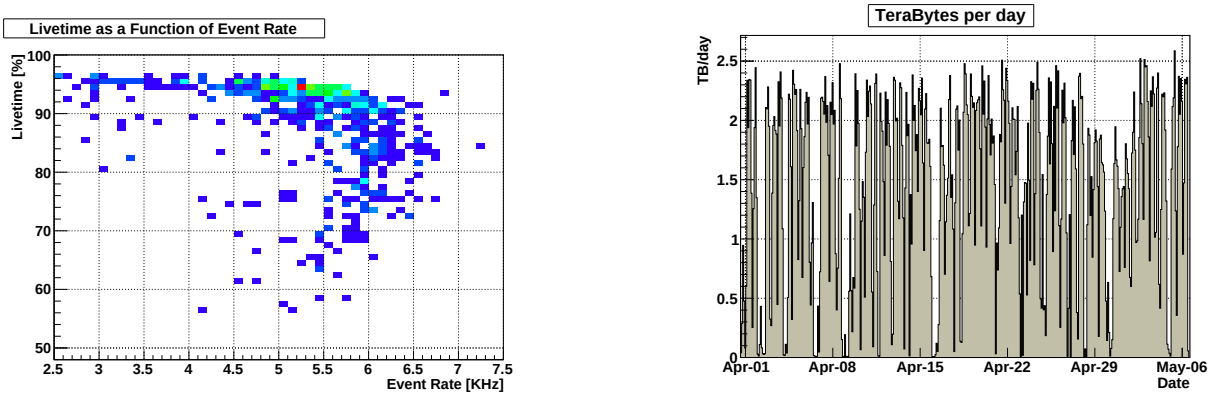

Figure 2.9: (left) The PHENIX data acquisition live time as a function of the total archive rate. (right) The acquired data volume in TeraBytes as a function of time, for each day since 4/1/2014.

The firmware upgrade of the GL1 eliminated a source of dead time in the trigger, which would occur when the GL1 sensed that all 5 readout buffers are filled, asserting a busy to the front-end modules. Instead of releasing the busy as soon as the first buffer was available, it previously waited until all buffers had been drained. The upgraded firmware now releases the busy as soon as the next buffer becomes available, leading to a decreased dead time, especially under high loads.

The data acquisition has various types of *Assembly and Trigger Processors* (ATPs). We decommissioned the oldest and slowest machines and replaced them with faster models. The ATPs assemble the events and perform the CPU-intensive compression of the raw data. The increased processing power allows a higher data throughput.

The main network switch was better tuned for the type of network traffic it actually handles. In addition, we were able to obtain spare parts from a switch in the RHIC Computing Facility which was replaced with a different model. This increased the number of available 10 Gigabit ports and allowed for a factor of two better connectivity to the HPSS storage system, and for selected machines to be connected with 10 Gigabit Ethernet.

Figure 2.9 (right panel) shows the data volume acquired per day for each day since 4/1/2014. We are on track to exceed an overall data volume of 3 TB in Run-14.

Chapter 3

Proposal for Run-15 and Run-16

In this section we provide details on the PHENIX collaboration beam use request, including the assumptions and inputs for luminosities and number of weeks for each request.

3.1 Accelerator performance and luminosity estimates

The physics performance evaluations in this document are based upon guidance provided by the Collider-Accelerator Department (C-AD) as documented in Ref. [1]. Also necessary are projections for the PHENIX experiment performance in terms of uptime and trigger sampling. We use the following values based on metrics from the experimental running over the last three years.

- The PHENIX uptime (the fraction of time when the beams are colliding that the PHENIX data acquisition is running and thus sampling physics) is 70%. This has been an area that PHENIX has placed particular emphasis on and observed consistent improvement.

- The PHENIX forward and barrel silicon vertex detectors have an optimal acceptance for collisions with z-vertex $|z| < 10$ cm. For other analyses in the central arm spectrometers not requiring the vertex detectors the acceptance is optimal for $|z| < 30$ cm. For the new MPC-EX forward measurements an even wider collision vertex range is utilized: $|z| < 40$ cm. We have labeled all physics projection integrated luminosities with the corresponding z-vertex range. Although the fraction of collisions within each selection varies somewhat with collision species, for these projections we assume that 70% of all collisions are within $|z| < 40$ cm, 60% of all collisions are within $|z| < 30$ cm, and 30% of all collisions are within $|z| < 10$. The one exception is for the proposed running at 62 GeV where the values are lower and are detailed explicitly later.

- The PHENIX data acquisition livetime is quite high — typically better than 90%.

All of this information is utilized and the values quoted in the performance figures are in terms of sampled integrated luminosity by PHENIX within the specified z-vertex range.

3.2 Run-15 request for $p+p$ @ 200 GeV with transverse polarization

The new capabilities of the MPC-EX upgrade and the interest in transverse spin physics drive our request for transversely polarized $p+p$ @ 200 GeV running. The running also provides additional statistics for all heavy ion baseline measurements. The large transverse single-spin asymmetries observed in polarized $p+p$ collisions at RHIC are believed to be related to a combination of initial and final state effects that originate primarily in the valence region of the projectile nucleon, the Sivers or transversity distributions in the transverse-momentum dependent TMD approach, or parton correlations in a collinear factorized framework. While data in semi-inclusive deep-inelastic scattering has been used to constrain these effects, the situation is more complicated in $p+p$ collisions due to the presence of both strong initial and final-state corrections arising from the soft exchange of gluons. Existing measurements at forward rapidity at RHIC in transversely polarized $p+p$ collisions are limited to hadronic observables, and therefore sample a number of different partonic processes. In contrast, direct photon production at forward rapidity is dominated by the scattering of a valence quark from the polarized projectile off a low-x gluon in the unpolarized proton.

Prompt photons at forward rapidities are roughly an equal mix of direct photons and photons from the fragmentation of the scattered valence quark. Theoretical studies indicate that the contribution from transversity and a polarized fragmentation function is small so that the single spin asymmetry for fragmentation photons largely carries the same information about the initial state of the polarized nucleon and reinforces the asymmetry from direct photons. A measurement of the single spin asymmetry for prompt photons will shed light on the mechanisms that produce asymmetries in forward hadron production in polarized $p+p$ collisions, and their relationship to the spin asymmetries measured in semi-inclusive deep-inelastic scattering (SIDIS). Because prompt photons are sensitive to "initial state" effects, such as the Sivers function, the measurement of a prompt photon A_N addresses NSAC milestone HP13.

The expected statistical precision from the MPC-EX measurement is shown in Figure 3.1, along with theory predictions from Kang et al. [26]. This figure includes contributions from direct and fragmentation photons, as well as the subtraction of the π^0 and η background asymmetries. The integrated luminosity request is driven by the requirement to make a definitive determination of the sign and pin down the magnitude at the $< 2\%$ level. The predicted sign of the asymmetry is different between extractions of the Sivers function

from SIDIS data and the twist-3 quark-gluon correlation function extracted from RHIC asymmetries. Measurement of a prompt photon asymmetry at RHIC will provide valuable insight into the different QCD methodologies applied to calculate these asymmetries.

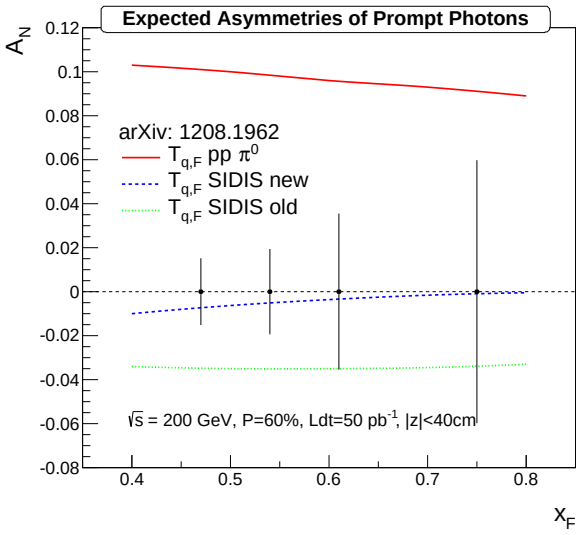

Figure 3.1: Projected sensitivity for the prompt photon single spin asymmetry with the MPC-EX assuming an integrated luminosity of 50 pb^{-1} and 60% beam polarization. The sensitivities are shown compared to calculations in the collinear factorized approach using a direct extraction of the quark-gluon correlation function from polarized $p+p$ data (upper solid red curve), compared to the correlation function derived from SIDIS extractions (lower dotted and dashed curves).

There are a number other measurements in transversely polarized $p+p$ collisions that can also be made with a 50 pb^{-1} data set, concurrent with the prompt photon measurement:

- Identified π^0 and η single spin asymmetries out to large transverse momentum (5–6 GeV/c)
- Measurement of the Interference Fragmentation Function (IFF) using hadron correlations (see Figure 3.2)
- Measurement of the contribution of the Collins fragmentation function to transverse single spin asymmetries through hadron correlations (both central + MPC as well as reconstruction of a jet axis in the MPC-EX)
- Measurement of heavy flavor A_N using single muons with improved background rejection with the FVTX detector (see Figure 3.3)

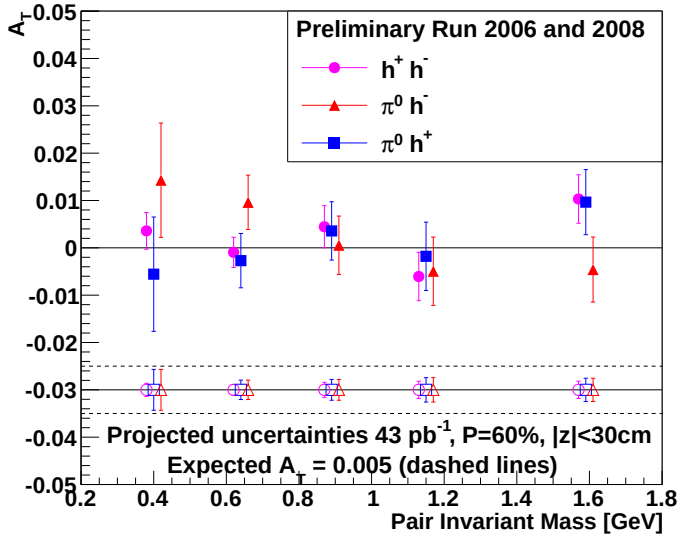

Figure 3.2: PHENIX preliminary results of interference fragmentation functions from Run-06 and Run-08. Shown are three different combinations of hadron pairs. Also shown are projections for the luminosity request in Run-15.

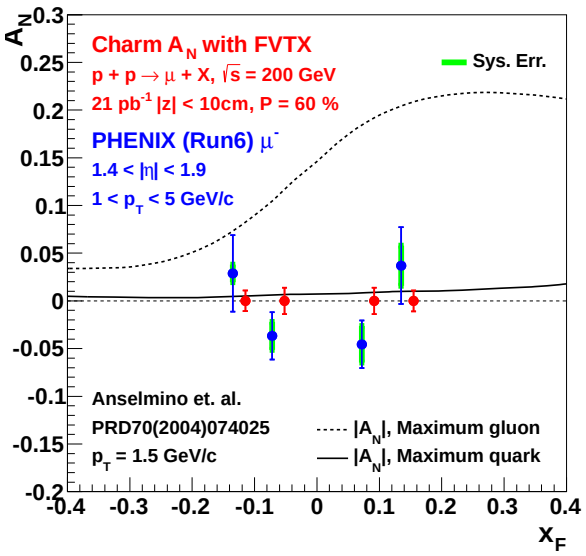

Figure 3.3: Single spin charm asymmetry, A_N, in transversely polarized $p+p$ @ 200 GeV.

3.3 Run-15 request for p+Au @ 200 GeV with transverse polarization

There are a number of very exciting opportunities with polarized p+A collisions enabled by accelerator advances and the new detector capabilities in PHENIX since the last d+Au @ 200 GeV data taking in 2008. We highlight these opportunities with physics projection plots in the following subsections.

The highest priority for this set of colliding systems is for a high statistics p+Au @ 200 GeV data set with a PHENIX integrated luminosity of 190 nb^{-1} within the z-vertex range $|z| < 40$ cm (the optimal acceptance range for the MPC-EX).

A key set of new observables utilize the polarization of the proton beam with a required 60% average transverse polarization. Since the accelerator has not run p+A systems before, we have estimated from other system ramp up times and the C-AD provided luminosity projections that this requires five weeks of physics running. This will provide an excellent p+Au data set of a number of key observables.

We believe it would be very beneficial to split the time evenly into p+Au and Au+p (i.e., reversing the beam directions). This was done with a two day turnaround for p+Pb to Pb+p running at the LHC. Comparing observables after swapping the p-going and Au-going directions provides a very useful way to understand and reduce systematic uncertainties in the measurement. We seek input from C-AD on the possible switching time and the implications on the delivered luminosities. We note that this was recommended by the PAC after last year's review.

We highlight below the great utility in having comparable statistical precision measurements in p+Si, which requires two weeks of physics running. As we argue below, there is sufficient reason to believe that additional nuclei would provide new insights that the door should remain open to the possibility of more p+A running in Run-16.

3.3.1 Polarized p+A: a unique test of saturation physics

The prospect of unique transverse polarized protons colliding with nuclei has generated a great deal of interest in the community — see the BNL-LANL-RBRC workshop talks for more details [27].

The MPC-EX enables an exciting new measurement proposed by Kang and Yuan [28]. It is predicted that the ratio of single spin asymmetries for neutral pions in p+A collisions to that in p+p collisions as a function of transverse momentum will be sensitive to the ratio of saturation scales the two systems, with the ratio suppressed below one when $p_T < Q_{\rm sat}^A$. A measurement of the asymmetry ratio as a function of transverse momentum for different nuclear species will elucidate if a saturation mechanism is a correct description of the underlying physics at low-x, and characterize its A dependence. It should be noted that

while this measurement borrows a technique from spin physics, the underlying physics measurement is directly related to cold nuclear matter. This represents a completely unique utilization of the excellent RHIC accelerator complex. Projected uncertainties with the requests p+Au and p+p @ 200 GeV transversely polarized running are shown in Figure 3.4. The addition of comparable statistical and systematic precision data in p+Si allow for a mapping out of this phenomenon. It may prove desirable in the future to consider additional intermediate nuclei.

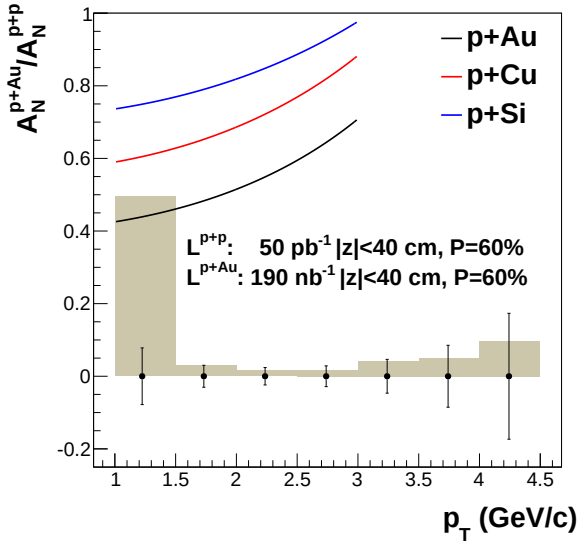

Figure 3.4: Shown are the projected statistical and systematic uncertainties for the requested polarized p+Au and p+p @ 200 GeV running. The colored curves represent a schematic expectation from the model of Kang and Yuan and apply for transverse momentum values below the saturation scale. These curves follow the functional form with the assumption that $Q_{\rm sat} = 1$ GeV/c and $Q^A_{\rm sat} = A^{1/3} Q_{\rm sat}$, plus a delta parameter related to the form of the Collins FF. The mapping out of the p_T and A dependence is thus very important.

3.3.2 Constraining the gluon nuclear PDF

One of the main physics goals of the MPC-EX is the characterization of the gluon distribution in nuclei at low-x. It has been known for some time that low-x gluons in nuclei are suppressed at small-x ($x \sim 10^{-3}$) compared to in protons, but the magnitude of this suppression is poorly constrained by existing experimental data. It has been conjectured that at low-x in the nucleus the gluon density saturates below a scale $Q_{\rm sat}$, forming a universal state known as the Color Glass Condensate. The existence of such a state would tame the rapid growth of the gluon PDF indicated by data from HERA DIS experiments, and there are tantalizing hints from RHIC d+Au collisions that such a state may be accessible at RHIC. Understanding the gluon distribution at low-x in nuclei is critical to a complete

understanding of the formation and evolution of the quark-gluon plasma in heavy-ion collisions.

Current probes of low-x at RHIC have relied on hadronic probes, which average over many partonic processes and only partially access the gluon distribution in nuclei. Effects of shadowing and anti-shadowing are clear from the PHENIX measurements to date of quarkonia and open heavy flavor leptons in d+Au collisions; however, that does not allow for a precision quantification. In contrast, prompt photon production at forward rapidities is dominated by q+g scattering in leading order, and is optimally sensitive to the gluon distribution. The MPC-EX will measure prompt photons in p+p and p+A collisions (with A $\in$ {Au, Si}) for $p_T > 3$ GeV/c to extract the ratio R_{pA}. This measurement will provide constraints on existing models of the gluon distribution at low-x, such as the EPS09 nuclear PDFs [29].

The difference between Si and Au is sufficiently large as to provide significant lever arm in most cold nuclear matter variables. In considering which lighter nucleus to utilize and whether only one additional nuclei is sufficient, we have compiled Monte Carlo Glauber parameters for a full range of targets as shown in Table 3.1. The distribution of the number of binary collisions is shown in Figure 3.5. For saturation physics, Si is a good choice in that the gluon density is still sufficient such that theoretical calculations indicate measurable effects. Another argument for a light nucleus is to confirm interesting preliminary findings from neutral pions and jets as measured in d+Au peripheral events [30]. The p + light ion allows one to remove any centrality categorization bias and also the complication of two projectile nucleons. In the 60-88% peripheral category of d+Au, the average number of binary collisions is $\langle N_{coll} \rangle = 3.2$. That might indicate an optimal comparison with p+Cu. However, for various physics effects related to multi-parton interactions and multiple initial and final state parton scattering, the more relevant number is the average number of binary collisions per projectile (i.e. deuteron) nucleon, which is closer to two, indicating p+Si as the optimal comparison. This highlights that running more than just two nuclei (Si and Au) might be insightful in future running.

For the requested data samples, we have projections for the statistical and systematic uncertainties on the direct photon measurement in p+A and p+p @ 200 GeV. To gauge the constraining power of these measurements on the gluon nuclear parton distribution function, we consider the suite of EPS09 nPDFs. We carry out a global fit and find the one and two standard deviation consistency bands. Shown in Figure 3.6 is the full set of current EPS09 gluon nPDFs as a function of x in Au and Si nuclei. Then highlighted in dark and light blue are the one and two standard deviation constraints from this direct photon MPC-EX measurement.

Additional constraints with charm and beauty production at forward and backward rapidity with the forward silicon vertex detector (FVTX) allow for consistency checks. The projected measurements from the FVTX with a fully unfolded flavor separation are shown in Figure 3.7. These measurements, along with comparable ones at midrapidty with the VTX, also provide a crucial baseline for the A+A heavy flavor results — in particular with

Table 3.1: Monte Carlo Glauber parameters for a range of targets of interest for p+A collisions at RHIC.

Element	A	$\langle N_{coll} \rangle$	$A^{1/3}$	$A^{1/3}/Au^{1/3}$	$A^{1/3}/Cu^{1/3}$
B	11	1.60	2.22	0.38	0.56
C	12	1.69	2.29	0.39	0.58
N	14	1.93	2.41	0.41	0.61
O	16	1.95	2.52	0.43	0.63
Ne	20	2.03	2.71	0.47	0.68
Na	23	-	2.84	0.49	0.71
Al	27	-	3.00	0.52	0.75
Si	28	2.35	3.04	0.52	0.76
Ar	40	-	3.42	0.59	0.86
Cu	63	3.00	3.98	0.68	1.00
Au	197	4.70	5.82	1.00	1.46

constraints on the Cronin effect and initial state parton energy loss.

Heavy quarkonia measurements in d+Au collisions have proven challenging to describe in terms of initial state nuclear modified parton distribution functions (nPDFs) and a simple nuclear break-up cross section [31, 32]. Extending these results to measurements in $p+A$ collisions with various nuclear targets A will add key independent checks on the geometric dependencies. Shown in Figure 3.8 are the projected uncertainties for J/ψ measurements for four different possible nuclear targets for the proposed integrated luminosities.

The momentum resolution improvement in the muon arms with the addition of the FVTX provides for the first time the ability to measure the ψ' at forward and backward rapidities. Figure 3.8 (right panel) shows the ψ' projected uncertainties. The centrality dependence of the ψ' as a function of rapidity will be a key test of models of charmonium production at different time scales and gluon densities [33].

One key item on all of these measurements to note is the emphasis on the geometry dependence. For example, nuclear modified PDFs are to date largely constrained from deep inelastic scattering from nuclei and thus average over the entire nucleus. Thus far,

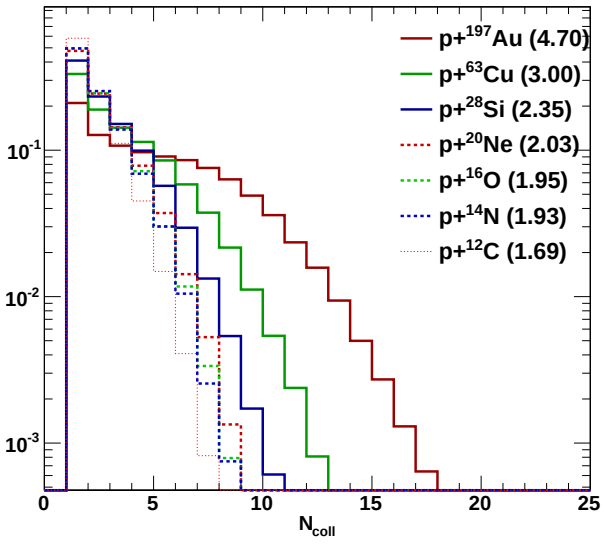

Figure 3.5: Distribution of the number of binary collisions calculated in a Glauber Monte-Carlo for p+A with various nuclear targets.

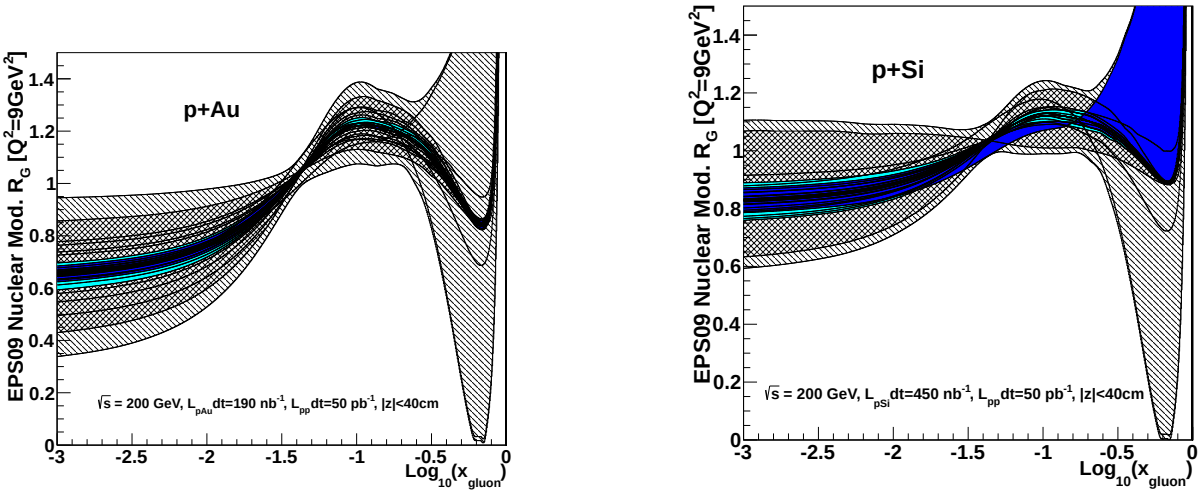

Figure 3.6: EPS09 nuclear parton distribution functions for gluons in Au (left) and Si (right) nuclei. The grey range shows the current band consistent with existing data. The dark blue and light blue bands show the one and two standard deviation constraints from the direct photon measurements proposed here.

RHIC results have selected different nuclear densities via centrality selection in d+Au collisions. These result in quantified systematic uncertainties, and for the highest transverse momentum jet and neutral pion results there are stronger additional auto-correlations with the centrality selections [8]. The ability to check these nuclear dependencies with minimum bias p+A with different nuclei is critical for pinning down how these effects depend on the nuclear density. These dependencies are a key to unlocking the underlying

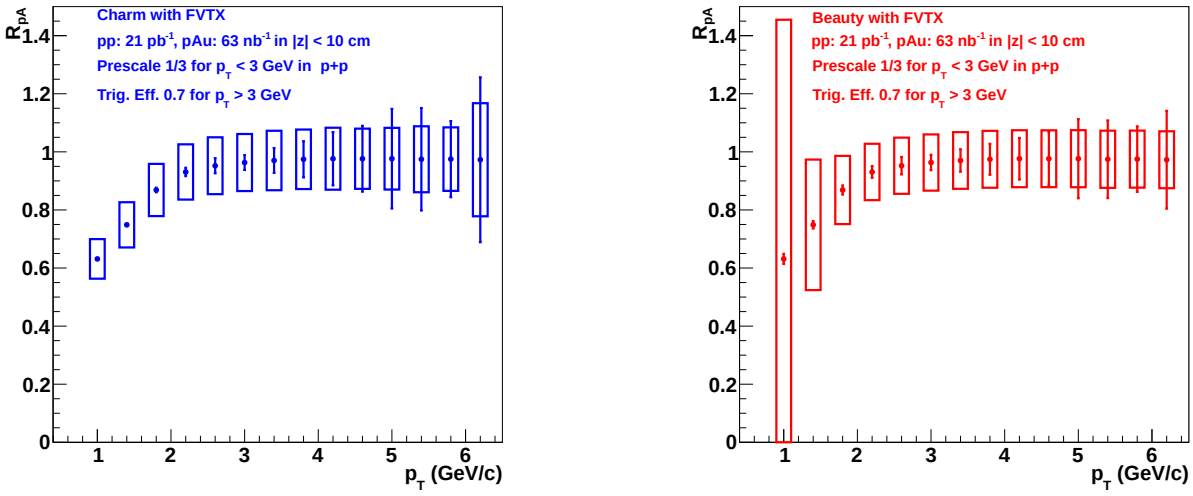

Figure 3.7: Projected uncertainties for R_{pA} for open charm (left) and open beauty (right) via the measurement of single muons with displaced verticies detected with the FVTX. The open boxes are systematic uncertainties that include contributions from the unfolding of the two heavy flavor components.

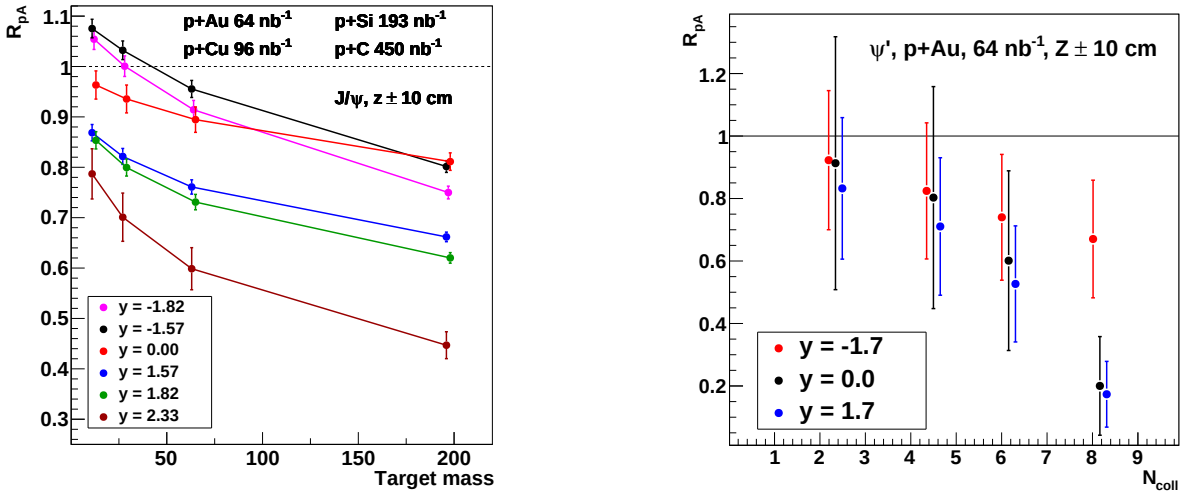

Figure 3.8: (left) Projected uncertainties for J/ψ R_{pA} and the possible nuclear and rapidity dependence from modeling of the d+Au measurements. (right) Projected uncertainties for the ψ' R_{pAu} at different rapidities from 64 nb^{-1}.

physics. As one specific example, a two week p+Si run will allow for a better statistics measurement of the nominal physics of neutral pions and jets than the peripheral selection d+Au result.

3.4 Run-16 request for $p+p$ and Au+Au @ 62 GeV

A unique ability of RHIC is to change the beam energy and thus scan quark-gluon plasma interactions above, near, and below the transition temperature. Recent measurements from our Run-10 Au+Au at 62 GeV data set indicate surprising results in the heavy flavor sector [34]. Measurements of open heavy flavor with the PHENIX silicon detectors in this system closer to the transition temperature, and thus potentially stronger early time coupling, should provide key new information on the quark-gluon plasma and flow of heavy quarks in medium. Additionally, the more steeply falling p_T spectra of charm quarks initially actually makes this probe more sensitive to flow effects.

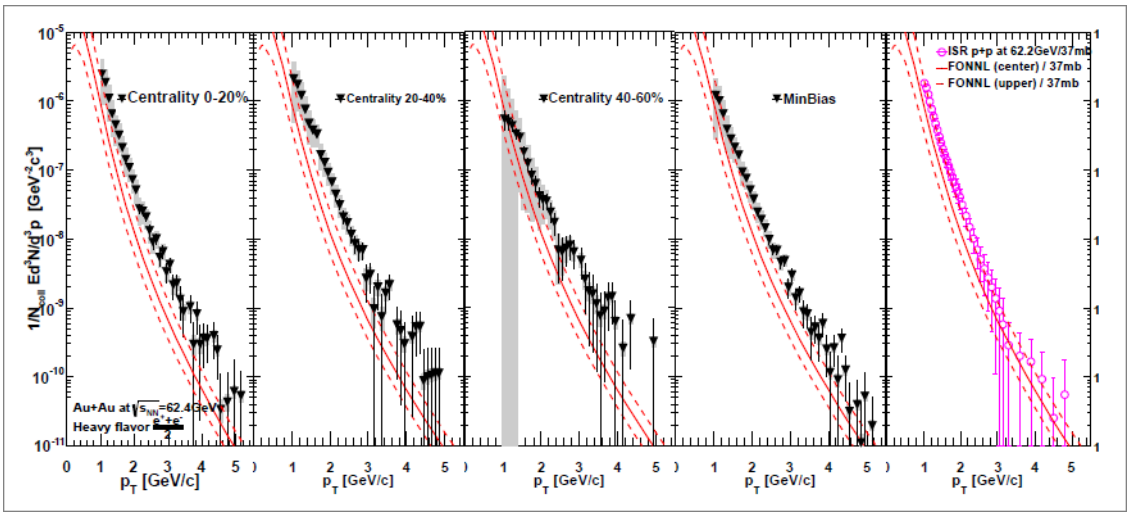

Figure 3.9: Shown are the measured non-photonic electron spectra from Au+Au collisions at 62 GeV for various centralities. In each selection, a comparison with binary scaled reference FONLL calculations are shown, detailed in the right most panel.

Figure 3.9 shows recently submitted PHENIX results on non-photonic electron spectra (measured prior to the installation of the silicon detectors) in Au+Au collisions at 62 GeV. Also, shown is the FONLL calculation as the $p+p$ baseline. One observes the Au+Au spectra being above the binary scaled $p+p$ references, i.e. $R_{AA} > 1$. This is strikingly different from measurements in Au+Au collisions at 200 GeV. Preliminary STAR measurements in Au+Au at 62 GeV indicate a similar enhancement effect [35]. We note that there is no RHIC measured $p+p$ reference data set and only older ISR measurements exist - as shown in Figure 3.10.

We have received additional guidance from C-AD on running conditions at this energy. Both the storage RF system and stochastic cooling work at this energy. Mike Blaskiewicz simulated the store luminosity for all cases, and the details are given in Table 3.2.

Following our standard running assumptions detailed earlier, this would result for Au+Au at 62 GeV in 3×10^9 PHENIX recorded events within the silicon detector acceptance of $|z| < 10$ cm with a 9 week running period. In a 6.5 week $p+p$ at 62 GeV run, the result

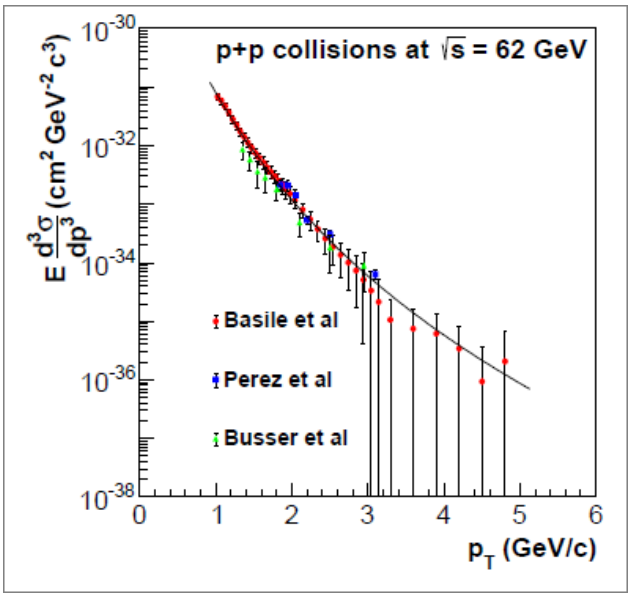

Figure 3.10: Shown are invariant yields of non-photonic electrons from three ISR publications for p+p collisoins at 62 GeV.

Table 3.2: C-AD providing information on p+p, p+A, Au+Au running at 62 GeV.

Collision System	Luminosity	L($\|z\| < 30$ cm)/Ltot	L($\|z\| < 10$ cm)/Ltot
Au+Au @ $\sqrt{s_{NN}} = 62$ GeV	400 μb^{-1}/week	45%	15%
p+p @ $\sqrt{s_{NN}} = 62$ GeV	2.1 pb^{-1}/week	23%	8%
p+Au @ $\sqrt{s_{NN}} = 62$ GeV	20 nb^{-1}/week	35%	12%

would be 3×10^{10} PHENIX trigger sampled events.

In fact, p+Au running at 62 GeV would be very interesting and a key additional constraint on the physics. We do not make it an explicit proposal only due to the constraints on Run-16 asymmetric species (i.e. p+A) running and the overall limit on cryo-weeks. If additional running time were available, even a short d+Au run at 62 GeV would be very interesting.

The above numbers indicate substantial data sets, and for example for Au+Au this would be much larger than the 400 million events from the Run-10 data set (which was prior to any of the PHENIX silicon vertex detectors being installed). These are smaller than data sets at 200 GeV and the total charm cross section is approximately a factor of 5 smaller at 62 GeV collision energy. Taking all of these factors into account, we show in Figure 3.11

the projected statistical uncertainties on the charm to electron nuclear modification factor R_{AA} and elliptic flow moment v_2.

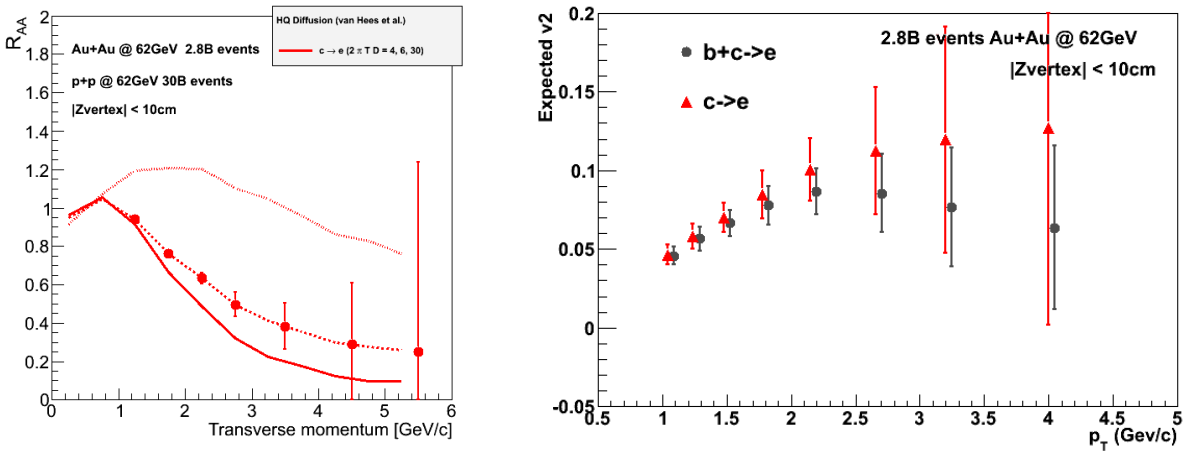

Figure 3.11: Shown are the projected uncertainties for the electrons from heavy flavor decay nuclear modification factor (left) and the flow coefficient v_2 (right). The theory curves are Au+Au 200 GeV predictions, and the modifications are expected to be significantly different.

We have contacted numerous theorists active in the study of heavy flavor production, modification, and medium interaction. There is a strong interest in this set of measurements. Shown in Figure 3.12 is a calculation from Ivan Vitev of the D meson nuclear modification factor in Au+Au at 62 GeV collisions compared with that in Au+Au at 200 GeV. The nuclear modifications are quite similar in this calculation with a modestly larger R_{AA} at lower p_T for the 62 GeV result. Also shown is a direct comparison of the PHENIX measurement heavy flavor electron R_{AA} and the calculation from Ivan Vitev, which indicates opposite trends, i.e. enhancement in the data and suppression in the theory.

Shown in Figure **??** are calculations from Ralf Rapp and collaborators for Au+Au at 62 GeV for the electron nuclear modification factor (left) and the elliptic flow parameter (right).

Another exciting physics measurement is that of thermal photons in Au+Au at 62 GeV. The comparison of the thermal photon emission between such a new measurement at 62 GeV and our published results at 200 GeV would be very illuminating. Many theoretical explanations that attempt to reconcile the Au+Au 200 GeV thermal photon yield and flow coefficients require stronger coupling near the transition temperature. These calculations should thus predict larger such effects when the early stage quark-gluon plasma is closer to the tranformation temperature.

The method that can be employed is via external conversions that are tagged by their location in the barrel silicon vertex detector. The same method was applied in the recently submitted analysis from conversions in the back-plane of the HBD. The overall combinatorial background is lower for Au+Au at 62 GeV and the pointing to the conversion location

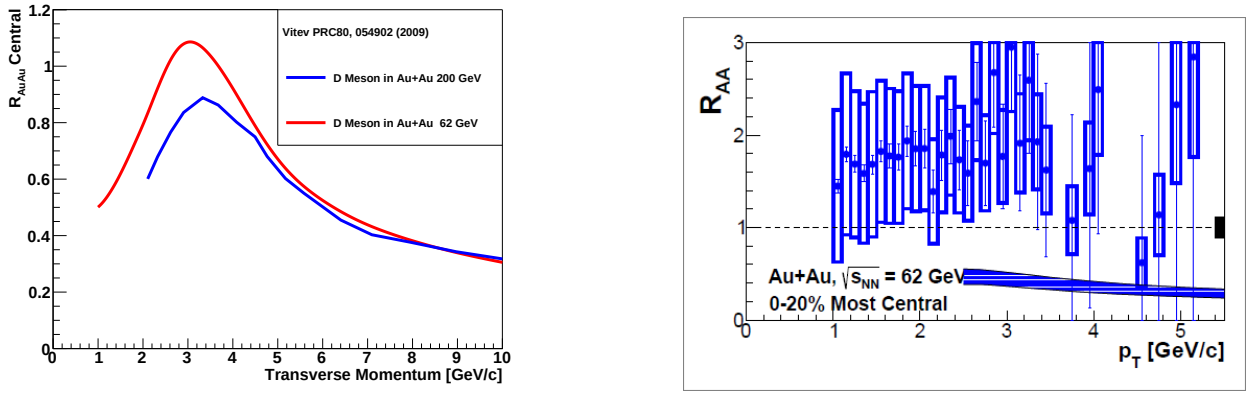

Figure 3.12: (Left) Shown is the nuclear modification factor prediction for D mesons in Au+Au collisions at 62 GeV and 200 GeV from Ivan Vitev. (Right) Shown is the PHENIX measurement heavy flavor electron R_{AA} as a function of transverse momentum in comparison with a calculation from Ivan Vitev. Note that the experimental uncertainties are highly correlated and dominated by the uncertainty in the p+p reference.

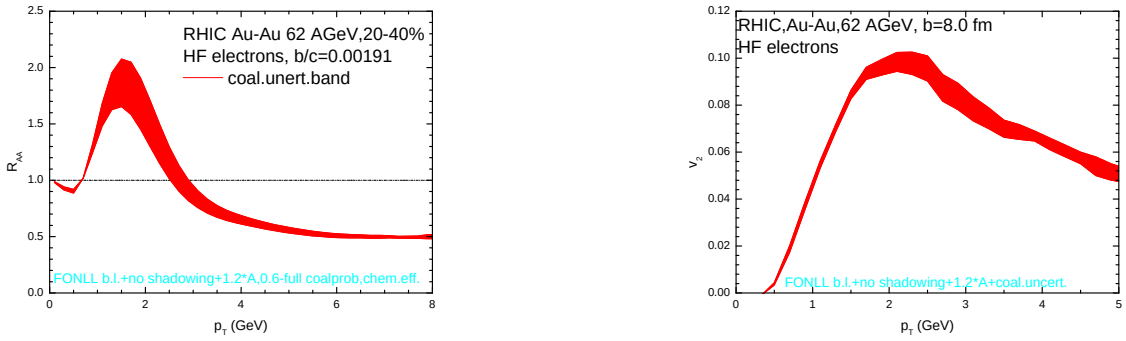

Figure 3.13: Shown are calculations from Ralf Rapp and collaborators for the heavy flavor electron nuclear modification factor (left) and the elliptic flow parameter (right).

in the VTX is good. We believe this is a key measurement for a full understanding of the quark-gluon plasma.

3.4.1 p+p @ 62 GeV with longitudinal polarization

The above requested p+p at 62 GeV would be with longitudinal polarization. At the higher p+p beam energies, the PHENIX neutral pion A_{LL} result [23] is most sensitive to the lower x range, in contrast to the higher x sensitivity of the STAR reconstructed single jet A_{LL}. Shifting the beam energy lower gives the PHENIX neutral pion measurement access to the higher x range where STAR has measured a non-zero double spin asymmetry. This would be an exciting opportunity to confirm this result in a different channel.

Results of double helicity asymmetry in inclusive jet production by STAR Collaboration [36] have indicated the non-zero contribution of gluon spin to the proton spin in the intermediate gluon momentum fraction x, as was shown by the recent DSSV global fit [37]. PHENIX π^0 A_{LL} data are consistent with this global fit result, though probing lower x our asymmetries are also consistent with $\Delta G = 0$ [23], demonstrating only limited sensitivity to ΔG in the region probed by STAR measurements. π^0 measurements at lower center of mass energy, $\sqrt{s} = 62.4$ GeV will provide us with good sensitivity to ΔG in the region probed by STAR's jets, and will serve as an important cross check of non-zero gluon polarization in the x range probed by RHIC data. Figure 3.14 combines the A_{LL} results from inclusive jet and π^0 measurements at $\sqrt{s} = 200$ GeV and PHENIX projections for π^0 A_{LL} at $\sqrt{s} = 62.4$ GeV, along with DSSV calculations based on the global fit of the world polarized data [37]. π^0 at $\sqrt{s} = 62.4$ GeV will probe gluon polarization in the x range probed by STAR's jet measurements at $\sqrt{s} = 200$ GeV but at lower scale set by the transverse momentum accessed. Hence, the comparison of these data sets also involves ΔG evolution.

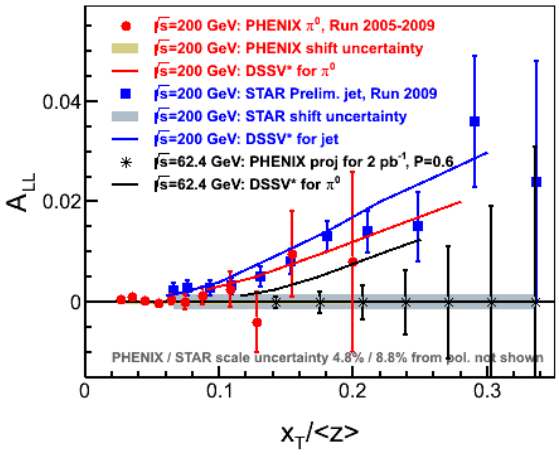

Figure 3.14: Preliminary STAR data for inclusive jets [36] and PHENIX data for inclusive π^0s [23] at $\sqrt{s} = 200$ GeV, and projections for π^0s at $\sqrt{s} = 62.4$ GeV for 2 pb^{-1} integrated luminosity sampled by PHENIX and 60% beam polarization; $< z >$=1 for jets and $< z >$=0.5 for π^0, to reflect that an individual pi0 carries only a fraction of the scattered parton momentum; curves are DSSV calculations based on the global fit [37], which includes $\sqrt{s} = 200$ GeV RHIC data shown in this plot.

3.5 Run-16 Considerations for Au+Au @ 200 GeV

The Run-14 Au+Au at 200 GeV run is currently projected (as shown in Figure 3.15) to exceed our beam use request of 1.5 nb^{-1} recorded by PHENIX within a z-vertex range

$|z| < 10$ cm. As detailed earlier, the silicon vertex barrel and forward detectors have been operating throughout with high efficiency and good acceptance. Our data acquisition is running at high rate and recording (not sampling) approximately 85% of all collisions within that z-vertex range when we are taking data. The steady high luminosity long stores delivered have also resulted in very high data taking efficiency as shown in Figure **??**. This Run-14 data sample when combined with the expected Run-15 p+p at 200 GeV data sample will represent our Golden Data Set for the study of open heavy flavor with the silicon detectors.

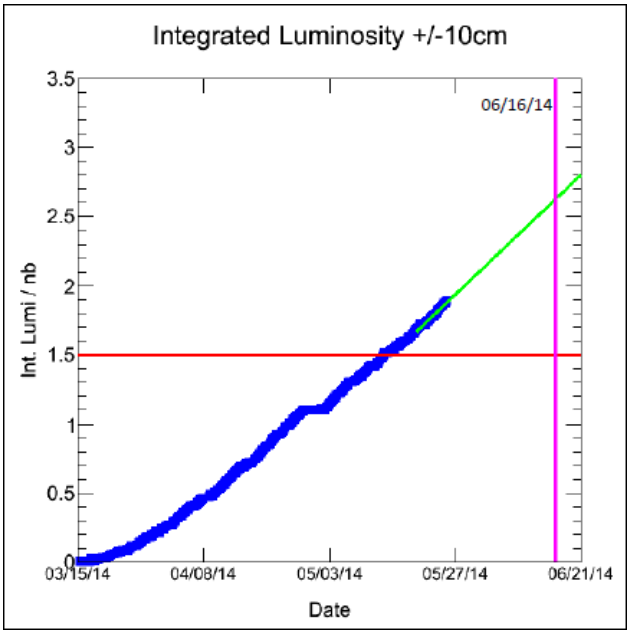

Figure 3.15: Run-14 Au+Au integrated luminosity to date compared with the Beam Use Proposal goal. We have already significantly exceeded the Beam Use Request physics goal for Au+Au at 200 GeV.

From the Beam Use Proposals last year, we understand that the STAR Collaboration will request additional Au+Au at 200 GeV running in Run-16. We address here the physics potential for PHENIX of this running. Note that the PHENIX detector will have essentially the same capabilities and acceptance as our Run-14 data taking (with the exception of the MPC-EX which operates only in lower occupancy p+p an p+A collisions).

The Run-14 beam conditions still have a somewhat wide z-vertex distribution, including satellite peaks as shown in Figure 3.17. From this typical distribution, one finds that 23% of all collisions occur within the optimal acceptance of the silicon detectors $|z| < 10$ cm, and 51% within $|z| < 30$ cm. If one excludes the satellite peaks, these values increase to 36% and 84% respectively. If the 56 MHz RF would be successful at capturing these satellite peaks into the main distribution, one could get a 50% increase in the rate within the tighter required z-vertex range. There are other optimizations being explored with C-AD that might result in slightly higher overall collision rates. These could be sampled with some increase in PHENIX data acquisition bandwidth (that might be achievable with some

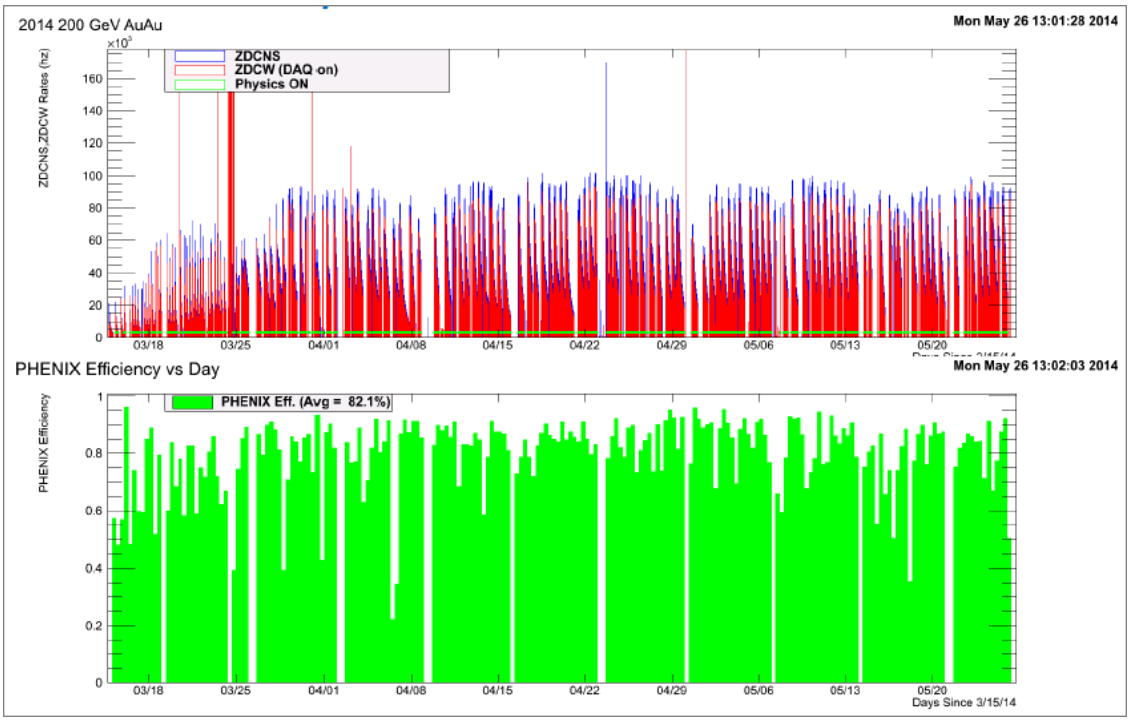

Figure 3.16: Graphical summary of the run performance for stores delivered and PHENIX data taking efficiency.

Event Builder upgrades and re-configuration), in addition to higher transverse momentum electrons and photons utilizing our ERT trigger.

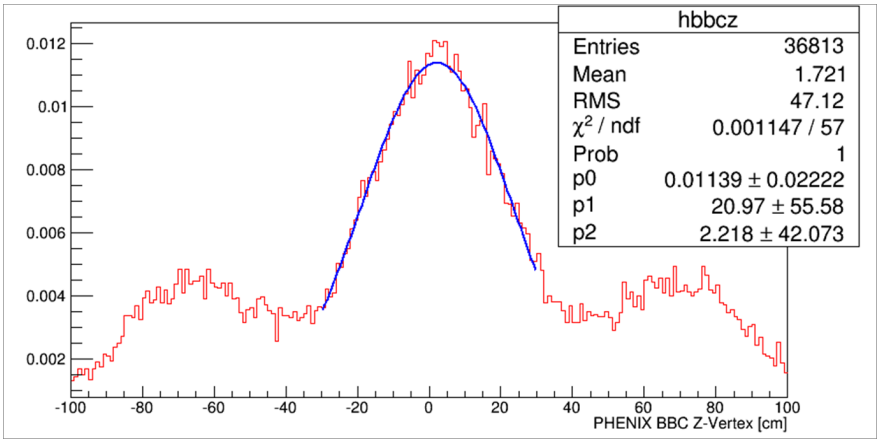

Figure 3.17: Run-14 Au+Au z-vertex distribution.

In an optimistic scenario, a ten-week physics run might result in a slightly larger data sample than that recorded in Run-14. If analysis from the Run-14 data set reveals particularly interesting results for higher p_T electrons, this factor of two increase in statistics could prove to be insightful.

3.6 Run-16 considerations for $p+p$ @ 510 GeV

We have also considered the possiblity of a several week 510 GeV polarized $p+p$ run in 2016. According to the C-AD projections about twice as much luminosity as in Run-13 can be accumulated in 10 weeks based on the average of minimum and maximum projections for Run-16. That said, the PHENIX forward muon channel measurements lose efficiency at higher colisions rates due to large Muon Identifier (MuID) currents, an effect that would be larger at higher luminosities. There are two possible physics goals which could be studied with 510 GeV running in Run-16.

Transverse polarization running for Drell-Yan Sivers function sign change

The modified universality of the Sivers function [38] and other transverse momentum dependent distribution functions results in a strong prediction of a sign change when compared to the one extracted in semi-inclusive DIS and Drell-Yan. As the Sivers function has been shown to exist by HERMES and COMPASS it is important to confirm this sign prediction in Drell-Yan or similar processes. This is the reason, some have proposed to study the transverse W single spin asymmetries by reconstructing the W transverse momentum. In PHENIX, the muon arms are needed to access an x_{Bj} range similar to that of SIDIS measurements. However, the conventional Drell-Yan mass range $4 < Q < 8$ GeV is likely very difficult to access due to substantial heavy flavor background and the limited statistical precision given a 10 week run. At best an indecisive data point could be extracted. That said, studies are ongoing to improve the feasibility of a conventional Drell-Yan in PHENIX.

Recently a new study has investigated the possibility to measure the Drell-Yan process in a mass range below the J/ψ at 2-2.5 GeV/c^2. This range would have the advantage, that the scales are also comparable with the SIDIS measurements and TMD evolution effects might be less of a concern and asymmetries as large as 8% could be expected. This very initial look at the low mass Drell-Yan which is based on Run-13 data claims to get heavy flavor and other backgrounds down to similar levels as the signal when applying high momentum selection criteria on the two muons. While this seems to remove much of the background it pushes the transverse virtual photon momentum above 1 GeV and the TMD formalism for describing these single spin asymmetries becomes not applicable. Acollinear approach would be needed and moves these measurements closer to the direct photon measurements planned in Run-15 with the MPC-EX.

Generally the TMD formalism is applicable only when there is a two-scale problem with one large scale Q and a substantially smaller transverse momentum scale Q_t of around the order of Λ_{QCD}. In the low mass Drell-Yan case, with large momentum cuts, both scales would be similar and already in the perturbative range and a collinear, higher twist description is more appropriate. Note, that while in the proposed W case, the two scales are rather different, they would still be both well within the perturbative regime as Ws with

transverse momenta below 1 GeV are difficult to constrain kinematically. The feasibility studies for high- and low-mass Drell-Yan are still in initial stages, and a clear statement is expected to be available for the actual Run-16 beam use proposal. Also theory input about what could be learned about Drell-Yan with a sizable transverse momentum in terms of the sign change is still necessary. Understanding in more detail how the transverse spin measurements of low mass Drell-Yan and Ws address the HP13 milestone require additional work.

Longitudinal polarization running for additional precision in the W A_L asymmetries

A second possibility would be to add to the Run-13 data set by running with longitudinal polarization to increase the statistics for forward $W \rightarrow \mu$ decays. Currently the obtained signal to background values are still not high enough to have small experimental uncertainties based on it. A larger data sample would allow to sacrifice more of the signal in favor of lower uncertainties related to the signal to background extraction. This would allow to better constrain the sea quark helicities and might also allow the study of a potential sign change of the d quark polarization at higher x. Such a sign change has been motivated by various theories based on the assumption, that in the limit of $x \rightarrow 1$ the total proton spin needs to accounted for by the struck parton alone. Its impact on the W asymmetries had been studied in the long version of the 2008 spin plan [39] and DSSV [40]. As can be seen in Figure 3.18 the additional statistics should make such a measurement possible. At the same time, efforts are being made to improve the overall W $\rightarrow \mu$ response of the muon arm detectors which could improve the sensitivity of the forward W measurements even further.

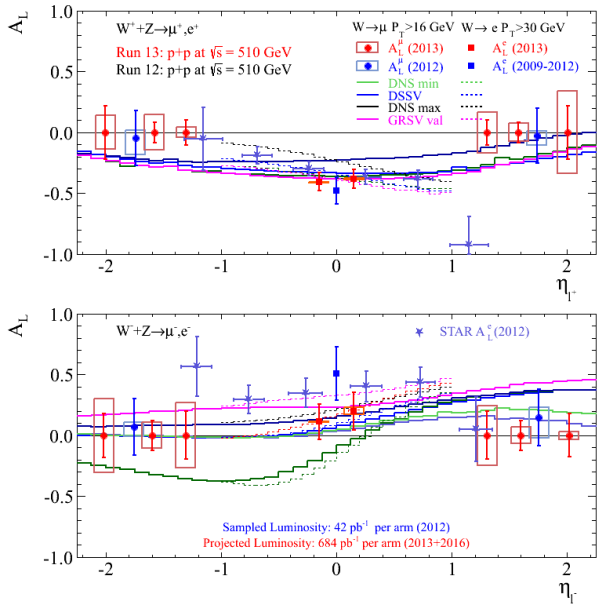

Figure 3.18: Uncertainty projections for W asymmetry measurements.

3.7 Run-16 request for RHICf

The RHICf collaboration has proposed to make a set of measurements using their very forward calorimeter detector (in front of the standard Zero Degree Calorimeters). The PHENIX collaboration finds this physics compelling and has agreed with work with them to integrate the device and collect the required data. The RHICf collaboration has prepared a separate full proposal based on C-AD input, and a brief summary is presented here for running this program in Run-16.

The motivations for RHICf are as follows:

- 1) to measure very forward particle production as critical input for high energy cosmic-ray physics programs. Measurements at RHIC in $p+p$ collisions at 510 GeV in conjunction with measurements at the LHC in $p+p$ collisions over the range 7-13 TeV make it possible to test Feynman scaling over a wide collision energy range.
- 2) Measurements with polarized $p+p$ collision using the RHICf detector allow a study of the forward particle asymmetry with a higher p_T resolution than the previous PHENIX measurements.
- 3) $p+$A collision to study the nuclear effect that is unavoidable to understand the cosmic-ray air shower.

The request included here assumes there is some form of $p+p$ running in Run-16 and thus a change to $p+p$ at 510 GeV and running the RHICf program in one week is feasible. The interest in $p+$A collisions would only be possible if there were a change in other constraints resulting in such running in Run-16. We note that the RHICf detector is not available for installation in PHENIX prior to Run-16.

If approved, the RHICf collaboration will bring one of the LHCf detectors to RHIC after the operation at the LHC in early 2015 is complete. The detector will be installed in front of one of the ZDCs in the PHENIX interaction hall. The detector will be held by a mechanism called a manipulator that allows the device to move vertically. This enables a scanning in pseudo-rapidity and evacuating to a stand-by position when RHICf does not take data so that RHICf does not interfere the ZDC operation. The data acquisition of RHICf is planned to be independent from PHENIX to reduce time for developing new electronics. The basic idea is to exchange triggers and identify common events between PHENIX and RHICf.

The running conditions for RHICf are described below, and have been discussed in detail with C-AD. Some constraints on the beam parameters are as follows: 1) low enough collision pile-up to avoid event overlap and low enough luminosity to avoid signal overlap in the slow scintillators, 2) high beta-star to define pseudo-rapidity of individual particle clearly, 3) horizontally polarized beam to observe asymmetry in wide p_T range vertically. To satisfy these constraints at 510 GeV $p+p$ collisions, RHICf proposes beam conditions as follows.

- E_{beam} = 255 GeV
- nb=111 bunches (including about 10 non-colliding bunches)
- I = 2×10^{11} protons/bunch
- $\beta^* = 10$ meters
- 1 day for physics operation plus 1 day for contingency
- Experimental commissioning can be performed when the RHICf detector is at the stand-by position and no dedicated beam time is required.
- According to RHIC Collider Projections (FY2014-FY2018) version 6 April estimated beam setup time In case the previous mode is polarized 255 GeV protons, 1–2 days. In case the previous mode is heavy ions, the setup time may be 4–5 days

RHICf is also interested in taking data at 200 GeV p+p and p+A collisions. In the case of p+A operation, RHICf needs to take data at the direction of proton beam that defines the installation at the south side of PHENIX. Again, these are not included in the current proposal here.

Appendix A

Beam use proposal charge

Date: Mon, Mar 10, 2014 at 4:38 PM

Dear RHIC Collaborations:

In view of the proximity of Quark Matter 2014 to the PAC meeting on June 11-13, the final version of the annual beam use proposals from the RHIC collaborations will be due on June 3, 2014. In view of the closeness of this date to the PAC meeting, and to leave the PAC members sufficient time to study the beam use requests, I urge you to not exceed this deadline. In order to permit Laboratory feedback before the proposals are finalized, I request that you send me a draft version of the beam use proposal no later than May 12, before everyone leaves for Quark Matter.

The proposals should describe and justify which beam operations you would like to see during the 2015 and 2016 runs, which are currently planned as 22 week runs. As usual, the beam use proposal should also give a brief review of recent published results and an early assessment of the success of Run-14.

Please send the proposals in electronic form to Peter Yamin, with copies to me, David Lissauer, Jamie Dunlop, and Thomas Roser.

Thanks in advance for your cooperation in this important matter.

Best regards

Berndt

Bibliography

[1] C-AD Run-14 and Run-15 Projection Document (provided by W. Fischer). URL: http://www.rhichome.bnl.gov/RHIC/Runs/RhicProjections.pdf. (document), 3.1

[2] J.L. Nagle, A. Adare, S. Beckman, T. Koblesky, J. Orjuela Koop, et al. Exploiting Intrinsic Triangular Geometry in Relativistic He3+Au Collisions to Disentangle Medium Properties. 2013. arXiv:1312.4565. (document)

[3] C. Aidala, N.N. Ajitanand, Y. Akiba, Y. Akiba, R. Akimoto, et al. sPHENIX: An Upgrade Concept from the PHENIX Collaboration. 2012. arXiv:1207.6378. (document)

[4] S.S. Adler et al. Transverse-energy distributions at midrapidity in p+p, d+Au, and Au+Au collisions at $\sqrt{s_{NN}} = 62.4$–200 GeV and implications for particle-production models. *Phys.Rev.*, C89:044905, 2014. arXiv:1312.6676, doi:10.1103/PhysRevC.89.044905. 1.1

[5] A. Adare et al. Measurement of long-range angular correlation and quadrupole anisotropy of pions and (anti)protons in central d+Au collisions at $\sqrt{s_{NN}}$=200 GeV. 2014. arXiv:1404.7461. 1.1

[6] A. Adare et al. Comparison of the space-time extent of the emission source in d+Au and Au+Au collisions at $\sqrt{s_{NN}} = 200$ GeV. 2014. arXiv:1404.5291. 1.1, 1.1

[7] A. Adare et al. Heavy-flavor electron-muon correlations in p+p and d+Au collisions at $\sqrt{s_{NN}}$ = 200 GeV. *Phys.Rev.*, C89:034915, 2014. arXiv:1311.1427, doi:10.1103/PhysRevC.89.034915. 1.1, 1.4

[8] A. Adare et al. Centrality categorization for $R_{p(d)+A}$ in high-energy collisions. 2013. arXiv:1310.4793. 1.1, 3.3.2

[9] A. Adare et al. Cold-nuclear-matter effects on heavy-quark production at forward and backward rapidity in d+Au collisions at $\sqrt{s_{NN}} = 200$ GeV. 2013. arXiv:1310.1005. 1.1

[10] A. Adare et al. Nuclear modification of ψ', χ_c and J/ψ production in d+Au collisions at $\sqrt{s_{NN}}$ = 200 GeV. *Phys.Rev.Lett.*, 111:202301, 2013. arXiv:1305.5516, doi:10.1103/PhysRevLett.111.202301. 1.1

[11] A. Adare et al. Spectra and ratios of identified particles in Au+Au and d+Au collisions at $\sqrt{s_{NN}} = 200$ GeV. 2013. arXiv:1304.3410. 1.1

[12] A. Adare et al. Cross section for $b\bar{b}$ production via dielectrons in d+Au collisions at $\sqrt{s_{NN}} = 200$ GeV. 2014. arXiv:1405.4004. 1.1, 1.4

[13] A. Adare et al. Measurement of K^0_S and K^{*0} in p+p, d+Au, and Cu+Cu collisions at $\sqrt{s_{NN}} = 200$ GeV. 2014. arXiv:1405.3628. 1.1

[14] Anne M. Sickles. Possible Evidence for Radial Flow of Heavy Mesons in d+Au Collisions. *Phys.Lett.*, B731:51–56, 2014. arXiv:1309.6924, doi:10.1016/j.physletb.2014.02.013. 1.1

[15] C. Aidala et al. Nuclear matter effects on J/ψ production in asymmetric Cu+Au collisions at $\sqrt{s_{NN}}$ = 200 GeV. 2014. arXiv:1404.1873. 1.2

[16] A. Adare et al. Centrality dependence of low-momentum direct-photon production in Au+Au collisions at $\sqrt{s_{NN}} = 200$ GeV. 2014. arXiv:1405.3940. 1.3

[17] A. Adare et al. Observation of direct-photon collective flow in $\sqrt{s_{NN}} = 200$ GeV Au+Au collisions. 2011. arXiv:1105.4126. 1.3

[18] Pierre Fayet. U-boson production in e+ e- annihilations, psi and Upsilon decays, and Light Dark Matter. *Phys.Rev.*, D75:115017, 2007. arXiv:hep-ph/0702176, doi:10.1103/PhysRevD.75.115017. 1.3

[19] A. Adare et al. Detailed measurement of the e^+e^- pair continuum in p+p and Au+Au collisions at $\sqrt{s_{NN}} = 200$ GeV and implications for direct photon production. *Phys. Rev.*, C81:034911, 2010. arXiv:0912.0244, doi:10.1103/PhysRevC.81.034911. 1.3

[20] L. Adamczyk et al. Dielectron Mass Spectra from Au+Au Collisions at $\sqrt{s_{\rm NN}}$ = 200 GeV. 2013. arXiv:1312.7397. 1.3

[21] A. Adare et al. Measurement of Υ(1S+2S+3S) production in p+p and Au+Au collisions at $\sqrt{s_{NN}} = 200$ GeV. 2014. arXiv:1404.2246. 1.4

[22] M. Strickland and D. Bazow. Thermal bottomonium suppression at RHIC and LHC. *Nucl. Phys.*, A879:25–58, 2012. arXiv:1112.2761, doi:10.1016/j.nuclphysa.2012.02.003. 1.7

[23] A. Adare et al. Inclusive double-helicity asymmetries in neutral pion and eta meson production in $\vec{p} + \vec{p}$ collisions at $\sqrt{s} = 200$ GeV. 2014. arXiv:1402.6296. 1.5, 3.4.1, 3.14

[24] A. Adare et al. Measurement of transverse-single-spin asymmetries for midrapidity and forward-rapidity production of hadrons in polarized p+p collisions at $\sqrt{s}$ =200 and 62.4 GeV. 2013. arXiv:1312.1995. 1.5

[25] C. Aidala et al. The PHENIX Forward Silicon Vertex Detector. *Nuclear Instruments and Methods in Physics Research A*, accepted for publication, 2014. arXiv:physics.ins-det/1311.3594v2. 2.1

[26] L. Gamberg and Z.-B. Kang. Single transverse spin asymmetry of prompt photon production. *Phys.Lett.*, B718:181–188, 2012. arXiv:1208.1962, doi:10.1016/j.physletb.2012.10.002. 3.2

[27] The Physics of p+A Collisions at RHIC. https://indico.bnl.gov/conferenceDisplay.py?ovw=True&confId=553, January 2013. 3.3.1

[28] Zhong-Bo Kang and Feng Yuan. Single Spin Asymmetry Scaling in the Forward Rapidity Region at RHIC. *Phys.Rev.*, D84:034019, 2011. arXiv:1106.1375, doi:10.1103/PhysRevD.84.034019. 3.3.1

[29] K. Eskola, H. Paukkunen, and C. Salgado. EPS09: a new generation of NLO and LO nuclear parton distribution functions. *JHEP*, 04:065, 2009. arXiv:0902.4154, doi:10.1088/1126-6708/2009/04/065. 3.3.2

[30] Baldo Sahlmueller. Cold Nuclear Matter Effects in d+Au Collisions at PHENIX. *Nucl.Phys.A904-905*, 2013:795c–798c, 2013. arXiv:1210.5547, doi:10.1016/j.nuclphysa.2013.02.136. 3.3.2

[31] A. Adare et al. Transverse-Momentum Dependence of the J/ψ Nuclear Modification in d+Au Collisions at $\sqrt{s_{NN}}$=200 GeV. 2012. arXiv:1204.0777. 3.3.2

[32] A. Adare et al. Cold Nuclear Matter Effects on J/ψ Yields as a Function of Rapidity and Nuclear Geometry in Deuteron-Gold Collisions at $\sqrt{s_{NN}} = 200$ GeV. *Phys.Rev.Lett.*, 107:142301, 2011. arXiv:1010.1246, doi:10.1103/PhysRevLett.107.142301. 3.3.2

[33] Francois Arleo and Stephane Peigne. Heavy-quarkonium suppression in p-A collisions from parton energy loss in cold QCD matter. *JHEP*, 1303:122, 2013. arXiv:1212.0434, doi:10.1007/JHEP03(2013)122. 3.3.2

[34] A. Adare et al. Heavy-quark production and elliptic flow in Au+Au collisions at $\sqrt{s_{NN}} = 62.4$ GeV. 2014. arXiv:1405.3301. 3.4

[35] Talk at the 30th Winter Workshop on Nuclear Dynamics, Barbara Trzeciak for the STAR Collaboration. URL: http://indico.cern.ch/event/275088/contribution/71/material/slides/0.pdf. 3.4

[36] Pibero Djawotho. Gluon polarization and jet production at STAR. 2013. arXiv:1303.0543, doi:10.1393/ncc/i2013-11569-3. 3.4.1, 3.14

[37] Daniel de Florian, Rodolfo Sassot, Marco Stratmann, and Werner Vogelsang. Evidence for polarization of gluons in the proton. 2014. arXiv:1404.4293. 3.4.1, 3.14

[38] J. Collins. Leading-twist single-transverse-spin asymmetries: Drell-Yan and deep-inelastic scattering. *Phys. Lett.*, B536:43–48, 2002. arXiv:hep-ph/0204004, doi:10.1016/S0370-2693(02)01819-1. 3.6

[39] Document: Plans for the RHIC Spin Program (June 2008). URL: http://spin.riken.bnl.gov/rsc/report/spinplan_2008/spinplan08.pdf. 3.6

[40] D. de Florian, R. Sassot, M. Stratmann, and W. Vogelsang. Extraction of Spin-Dependent Parton Densities and Their Uncertainties. *Phys. Rev.*, D80:034030, 2009. arXiv:0904.3821, doi:10.1103/PhysRevD.80.034030. 3.6